

# Hybrid of representation learning and reinforcement learning for dynamic and complex robotic motion planning

Chengmin Zhou<sup>a,b</sup>, Xin Lu<sup>c</sup>, Jiapeng Dai<sup>d</sup>, Xiaoxu Liu<sup>c</sup>, Bingding Huang<sup>d,\*</sup>, Pasi Fränti<sup>e,\*</sup>

<sup>a</sup> University of Eastern Finland FI-80100 Joensuu, Finland

<sup>b</sup> Shenzhen Technology University 518118 Shenzhen, China

<sup>c</sup> Sino-German College of Intelligent Manufacturing, Shenzhen Technology University, 518118 Shenzhen, China

<sup>d</sup> College of Big Data and Internet, Shenzhen Technology University, 518118 Shenzhen, China

<sup>e</sup> Machine Learning Group, School of Computing, University of Eastern Finland, FI-80100 Joensuu, Finland

## ARTICLE INFO

### Keywords:

Motion planning

Navigation

Reinforcement learning

Representation learning

Intelligent robot

## ABSTRACT

Motion planning is the soul of robot decision making. Classical planning algorithms like graph search and reaction-based algorithms face challenges in cases of dense and dynamic obstacles. Deep learning algorithms generate suboptimal one-step predictions that cause many collisions. Reinforcement learning algorithms generate optimal or near-optimal time-sequential predictions. However, they suffer from slow convergence, suboptimal converged results, and unstable training. This paper introduces a hybrid algorithm for robotic motion planning: *long short-term memory* (LSTM) and skip connection for attention-based discrete soft actor critic (LSA-DSAC). First, graph network (relational graph) and attention network (attention weight) interpret the environmental state for the learning of the discrete soft actor critic algorithm. The expressive power of attention network outperforms that of graph in our task by difference analysis of these two representation methods. However, attention based DSAC faces the problem of unstable training (vanishing gradient). Second, the skip connection method is integrated to attention based DSAC to mitigate unstable training and improve convergence speed. Third, LSTM is taken to replace the sum operator of attention weight and eliminate unstable training by slightly sacrificing convergence speed at early-stage training. Experiments show that LSA-DSAC outperforms the state-of-the-art in training and most evaluations. Physical robots are also implemented and tested in the real world.

## 1. Introduction

Intelligent robots play an important role in our daily life. For example, autonomous robot has been applied to hotel guidance [1], parcel delivery [2,3], and robotic arms in manufacturing [4,5]. Motion planning or path planning is the soul of robotic decision making. It enables robots to reach the goal and finish the tasks.

Classical planning algorithms like graph search (e.g., A\* [6] and Dijkstra's algorithm [7]) and sampling-based algorithms (e.g., rapidly

exploring random tree (RRT) [8] and probabilistic roadmap method (PRM) [9]) enable robots to navigate in static and dynamic environment. However, they cause many collisions in the environment with dense and dynamic obstacles because of the huge burden in updating the environmental map and sampling the environment information in real time.

Classical reaction-based algorithms like *dynamic window approach* (DWA) [10] and *optimal reciprocal collision avoidance* (ORCA) [11] reduce collisions in the environment with dense and dynamic obstacles

*List of abbreviations:* Long short-term memory, (LSTM); LSTM and skip connection for attention-based discrete soft actor critic, (LSA-DSAC); dynamic window approach, (DWA); Deep learning algorithms, (DL); reinforcement learning, (RL); advantage actor critic, (A2C); Monte-Carlo tree search, (MCTS); proximal policy optimization, (PPO); twin delayed deep deterministic policy gradient, (TD3); relational graph based DSAC, (RG-DSAC); skip connection for attention-based DSAC, (SA-DSAC); multi-layer perceptron, (MLP); robot operation system, (ROS); rapidly exploring random tree, (RRT); probabilistic roadmap method, (PRM); optimal reciprocal collision avoidance, (ORCA); convolutional neural network, (CNN); deep Q network, (DQN); asynchronous advantage actor critic, (A3C); deep deterministic policy gradient, (DDPG); soft actor critic, (SAC); relational graph, (RG); attention weight based DSAC, (AW-DSAC); Markov decision process, (MDP); local area network, (LAN); pulse-width modulation, (PWM).

\* Corresponding authors.

*E-mail addresses:* [zhou@cs.uef.fi](mailto:zhou@cs.uef.fi) (C. Zhou), [luwenkai67109@outlook.com](mailto:luwenkai67109@outlook.com) (X. Lu), [jalaxy1996@outlook.com](mailto:jalaxy1996@outlook.com) (J. Dai), [liuxiaoxu@sztu.edu.cn](mailto:liuxiaoxu@sztu.edu.cn) (X. Liu), [huangbingding@sztu.edu.cn](mailto:huangbingding@sztu.edu.cn) (B. Huang), [franti@cs.uef.fi](mailto:franti@cs.uef.fi) (P. Fränti).

<https://doi.org/10.1016/j.robot.2025.105167>

Received 7 May 2024; Received in revised form 12 January 2025; Accepted 13 August 2025

Available online 14 August 2025

0921-8890/© 2025 The Author(s). Published by Elsevier B.V. This is an open access article under the CC BY license (<http://creativecommons.org/licenses/by/4.0/>).

because they compute robot's motion by just considering obstacle's geometry and speed information. This requires fewer information updates compared to the map update. However, high collision rates still exist in reaction-based algorithms when the robot avoids obstacles with high speed because of the increasing burden in the information update.

*Deep learning algorithms* (DL) like *convolutional neural network* (CNN) [12] avoid the information update problem of the reaction-based algorithms by training a model that generates robot's decisions or actions in real time. However, decisions from DL are based on one-step predictions which result in suboptimal trajectories when the robot moves toward its goals.

*Reinforcement learning* (RL) algorithms like *deep Q network* (DQN) [13] and *advantage actor critic* (A2C) or *asynchronous advantage actor critic* (A3C) [14] improve the one-step predictions of CNN by training the models based on the multi-step time-sequential predictions. These multi-step time-sequential predictions are better than the one-step predictions because the training of the RL model considers the time-sequential information of the goals and obstacles. RL, however, may suffer from slow convergence speed and suboptimal converged result once the input (the environment state) is low-quality with limited expressive power.

Currently, representation learning or deep learning methods LSTM [15], graph network [16,17], attention network [18,19], and tree search model (e.g., Monte-Carlo tree search (MCTS) [20]) improve the expressive power of input. RL algorithms are also improved by introducing new architectures. For optimal value based RL, double Q network architecture, dueling architectures, and energy-based architecture are introduced to improve the convergence, thus resulting in double deep Q networks [21], dueling deep Q network [22], and soft Q learning [23]. For actor-critic based RL, multi-thread architecture, deterministic architecture, monotonous architecture, and energy-based architecture are introduced to improve the convergence, thus resulting in the advantage actor critic [14], deep deterministic policy gradient (DDPG) [24,25], proximal policy optimization (PPO) [26], and soft actor critic (SAC) [27–29]. The fused architecture of the double Q networks and the actor-critic network is proved to be one of the most efficient architectures in RL [30]. This architecture is also applied to many RL variants, resulting in the *Twin delayed deep deterministic policy gradient* (TD3) [31] and SAC. The combination of representation learning and RL is a promising direction for better motion planning performance, because RL is fed with the input with high expressive power. This improves the overall convergence of RL algorithms.

**Optimizations and contributions.** Here, we first list the briefly describe RG-DSAC, AW-DSAC, SA-DSAC, and LSA-DSAC to make readers better understand following contents:

- **RG-DSAC:** relational graph based DSAC. This is the combination of relational graph (RG) and discrete action for soft actor critic (DSAC).
- **AW-DSAC:** attention weight based DSAC. This is the combination of attention network and DSAC. Here the attention weight (AW) is the weight of attention network, and attention weight can be used to compute attention score that provide better interpretability to indicate how important the dynamic obstacle is.
- **SA-DSAC:** skip connection for AW-DSAC. Here the skip connection is integrated into the attention network of AW-DSAC.
- **LSA-DSAC:** LSTM and skip connection for AW-DSAC. Here LSTM replaces the sum operator of attention network in SA-DSAC.

This paper targets improving motion planning performance of the robot among dense and dynamic obstacles by combining the representation learning and RL. We first implemented DSAC which is the soft actor critic algorithm in the setting of discrete action space and is also one of most efficient RL algorithms currently. DSAC is then combined with RG [16], resulting in the RG-DSAC that achieves satisfactory performance in motion planning. However, we found that the expressive power of the relational graph is limited in the experiment. The relational

graph just partly describes the relationship between the robot and obstacles via establishing the relationships for all agents without precisely focusing on the relationship between the robot and obstacles. This may result in the limited expressive power of interpreted environmental state. The expressive power of interpreted environmental state is improved by replacing the relational graph using AW [18] which precisely and explicitly analyze and describe the relationship between the robot and obstacles. This results in AW-DSAC which outperformed RG-DSAC in the early-stage training but suffered from unstable training. After analysis, we concluded that the *feature loss* and *pooling method* in attention network under deep network architecture may cause the unstable training. Hence, we optimized attention network by integrating the skip connection method and LSTM into the architecture of the attention network, resulting in SA-DSAC and LSA-DSAC. SA-DSAC mitigated the problem of unstable training improved convergence, while LSA-DSAC eliminated unstable training by sacrificing the convergence speed slightly at the early-stage training and overall convergence is improved consequently.

Overall, our work addresses unique challenges of maintaining interpretability, training stability, and efficiency simultaneously for dynamic complex robotic motion planning by optimizing attention network and combining it with efficient DSAC. Given our knowledge, we've never seen this from existing works, and it distinguishes our work from the state-of-the-arts.

The workflow is shown in Fig. 1. First, environment features are collected from circle-crossing simulator to feed RL algorithms for training. Second, we implement RG-DSAC and AW-DSAC which work as the baseline algorithms for comparisons. Third, we improve AW-DSAC, resulting in SA-DSAC and LSA-DSAC. The convergence of mentioned algorithms are compared by observing their training curves. Finally, physical implementation is done and robots are tested in dense and dynamic scenarios. Main contributions of this paper include:

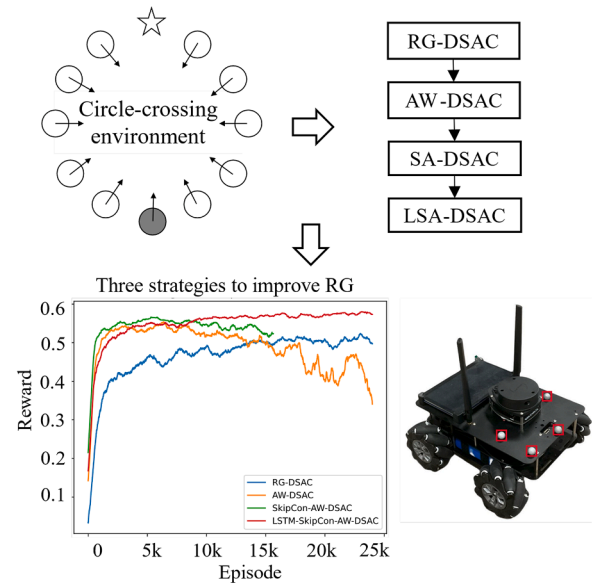


**Fig. 1.** Workflow of our LSA-DSAC. The training data is collected from the circle-crossing simulator. The RG-DSAC is implemented and selected as the trainable baseline algorithm for comparisons. Relational graph is replaced the attention weight (or attention network), resulting in AW-DSAC. The skip connection is applied to the attention network to improve the convergence, resulting in SA-DSAC. Finally, LSTM is applied to the SA-DSAC to further improve the convergence, resulting in LSA-DSAC. The training curves demonstrate a good convergence of LSA-DSAC over the rest algorithms. This paper includes the physical implementation which demonstrates how to transplant our algorithm into the real world. Our test code is available on website <https://github.com/CHUENGMINCHOU/LSA-DSAC>.

- 1) The implementation of RG-DSAC and AW-DSAC;
- 2) The LSA-DSAC which is the optimized version of AW-DSAC by integrating the skip connection method and LSTM into the architecture of the attention network of AW-DSAC;
- 3) Extensive evaluations of our algorithms against the state-of-the-arts;
- 4) Physical implementation, testing of the robot in real world, and analytical discussions about the problem of vanishing gradient in deep networks.

This paper is arranged as follows: Section II presents the state-of-the-art, problem formulation and preliminary of RL and DSAC. Section III presents RG-DSAC, AW-DSAC, SA-DSAC and LSA-DSAC. Section IV presents network framework of LSA-DSAC, model trainings, model evaluations and physical implementation. Section V provides discussions for unstable training and potential challenges.

## 2. Research background

This section first presents the state-of-the-art for dynamic robotic motion planning tasks. Then, the problem formulation of motion planning tasks is given by mathematic descriptions. Finally, the preliminary of RL and DSAC are presented. They are fundamental concepts for following further algorithm implementations and optimizations.

### 2.1. Technical difficulties of state-of-the-art for indoor motion planning among dense and dynamic scenarios

This paper focuses on RL-based methods to solve indoor robotic motion planning problems among dense and dynamic scenarios. The combination of representation learning and RL is promising for improving robotic motion planning performance. However, current works in this direction are still not good enough for challenging commercial tasks. Existing works about the combination of the representation learning and RL include the *relational graph based DQN* [16], *proximal policy optimization* with multiple robots [32], CADRL [33], LSTM-A2C [34,35], LSTM-RL [18] and SARL [18].

Relational graph based DQN is the combination of relational graph and DQN. Relational graph describes the relationship of all agents (the robot and obstacles), instead of focusing on the robot-obstacle relationship. Relational graph partly and indirectly represents the robot-obstacle relationship; therefore, its expressive power is limited. DQN faces over-estimation problems which cause the slow and suboptimal convergence of overall networks.

PPO with multiple robots faces problems of data quality because it learns obstacle features from entire source environmental state without precisely and explicitly analyzing the relationship between the robot and obstacles. Moreover, the entire source environmental state is interpreted by the CNN in the PPO with multiple robots. Background noise is also included in this interpretation process, resulting in poor quality of interpreted environmental state.

CADRL learns the pairwise feature of the robot and one obstacle by DQN. Then, a trained model is applied to the multiple-obstacle case. CADRL is myopic because it does not consider the relationship between the robot and obstacle. The closest obstacle feature is just used for training instead of all obstacle features. DQN in CADRL also brings high bias and variance.

In LSTM-A2C and LSTM-RL, LSTM encodes obstacle features by distance-based order which partly represents robot-obstacle relationship, resulting in limited expressive power of interpreted environmental state. A2C/A3C lack efficient data replay strategies, resulting in a slow convergence. A2C/A3C and DQN in LSTM-A2C and LSTM-RL bring high bias and variance, resulting in a slow convergence.

SARL consists of an attention network and DQN where attention network interprets robot-obstacle features to the attention weight that better describes the relationship between the robot and obstacles, resulting in the improvement of expressive power. However, attention

network still faces the problem of unstable training if overall architecture has deep and complex networks. Moreover, DQN brings high bias and variance. These two reasons cause the slow and suboptimal convergence of SARL.

### 2.2. Problem formulation

This paper focuses on the problem of indoor robotic motion planning defined by [11] and further maintains interpretability, training stability, and efficiency simultaneously for robotic motion planning by optimizing attention network and combining it with efficient DSAC. The state-of-the-arts presented in Section 2.1 just consider a part of these factors, resulting in their poor performance in either interpretability, training stability, or training/motion planning efficiencies. All algorithms including our algorithms and the state-of-the-art are trained and tested in simulators (Fig. 2) provided by ORCA [11]. Simulators includes *circle-crossing* and *square-crossing* simulators that add *predictable complexity* to the motion planning tasks. The objective of robotic motion planning is to navigate the robot to its destination and avoid all dense and dynamic obstacles. Consequently, the robot can arrive at its destination safely and efficiently. Detailed problem formulation is described as the follows:

Let  $a$  and  $v$  represent the action and velocity of robot where  $a = v = [v_x, v_y]$ . Let  $p = [p_x, p_y]$  represent the robot position. Let  $s_t$  represent the robot state at time step  $t$ .  $s_t$  consists of observable and hidden parts  $s_t = [s_t^{obs}, s_t^h]$ ,  $s_t \in R^9$ . Observable part refers to factors that can be measured or observed by others. It consists of the position, velocity, and radius  $s_t^{obs} = [p_x, p_y, v_x, v_y, r]$ ,  $s_t^{obs} \in R^5$ . The hidden part refers to factors that cannot be seen by others. It consists of planned goal position, preferred speed and heading angle  $s_t^h = [p_{gx}, p_{gy}, v_{pref}, \theta]$ ,  $s_t^h \in R^4$ . The state, position, and radius of the obstacles are described by  $\hat{s}$ ,  $\hat{p}$  and  $\hat{r}$  respectively.

We first introduce one-robot one-obstacle case, and then the one-robot multi-obstacle case. The robot plans its motion by the policy  $\pi : (s_{0:t}, \hat{s}_{0:t}^{obs}) \rightarrow a_t$  where  $s_{0:t}$  and  $\hat{s}_{0:t}^{obs}$  are the robot states and observable obstacle states from time step 0 to time step  $t$ , while the obstacles plan their motions by  $\hat{\pi} : (\hat{s}_{0:t}, s_{0:t}^{obs}) \rightarrow a_t$  where  $\hat{s}_{0:t}$  and  $s_{0:t}^{obs}$  are the obstacle states and observable robot states from time step 0 to time step  $t$ . The robot's objective is to minimize the expectation (average) of the time to its goal  $E[t_g]$  (Eq. (1)) under the policy  $\pi$  without collisions to the obstacles. The constraints of robot's motion planning can be formulated via (Eq. (2)–5) that represent the *collision avoidance constraint*, *goal constraint*, *kinematics of the robot* and *kinematics of the obstacle*, respectively. Collision avoidance constraint denotes that the distance of robot and obstacles  $\|p_t - \hat{p}_t\|_2$  should be greater than or equal to the radius sum of the robot and obstacles  $r + \hat{r}$ . Goal constraint denotes that the position of the robot  $p_{t_g}$  should be equal to the goal position  $p_g$  if the robot reaches its goal. Kinematics of the robot denotes that the robot position  $p_t$  is equal to the sum of robot position  $p_{t-1}$  and the change of the robot position  $\Delta t \cdot \pi : (s_{0:t}, \hat{s}_{0:t}^{obs})$ . The robot policy  $\pi : (s_{0:t}, \hat{s}_{0:t}^{obs})$  is a velocity decided by learning from historical robot states and obstacle states. Kinematics of the obstacle is the same as that of the robot.  $\hat{\pi} : (\hat{s}_{0:t}, s_{0:t}^{obs})$  is a velocity decided by the obstacle policy  $\hat{\pi}$  like ORCA.

$$\text{minimize } E[t_g | s_0, \hat{s}_0^{obs}, \pi, \hat{\pi}] \text{ s.t.} \quad (1)$$

$$\|p_t - \hat{p}_t\|_2 \geq r + \hat{r} \quad \forall t \quad (2)$$

$$p_{t_g} = p_g \quad (3)$$

$$p_t = p_{t-1} + \Delta t \cdot \pi : (s_{0:t}, \hat{s}_{0:t}^{obs}) \quad (4)$$

$$\hat{p}_t = \hat{p}_{t-1} + \Delta t \cdot \hat{\pi} : (\hat{s}_{0:t}, s_{0:t}^{obs}) \quad (5)$$

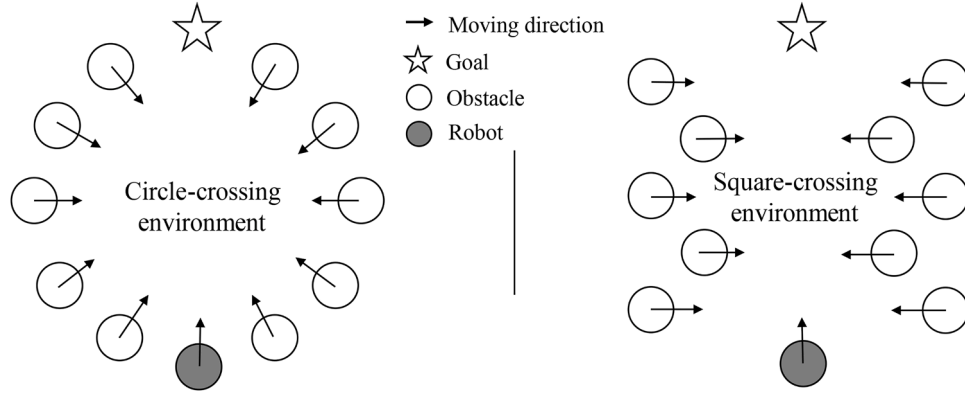


**Fig. 2.** Circle-crossing and square-crossing simulators. Obstacles are randomly generated near the brink of the circle in a circle-crossing environment. Then they move toward their opposite side. In the square-crossing environment, obstacles are randomly generated on the left side or right side and then they move toward random positions on their opposite side. The objective of the robot is to navigate itself from the start to the destination by controlling or planning its motions. This is achieved by controlling the robot with RL algorithms. The circle-crossing simulator is for training and testing simultaneously, while the square-crossing simulator is only for testing in the extensive evaluations.

In one-robot  $N$ -obstacle case, the objective is replaced by  $\text{minimize } E[t_g | s_0, \{\hat{s}_0^{obs} \dots \hat{s}_N^{obs}\}, \pi, \hat{\pi}]$  where we assume that obstacles use the same policy  $\hat{\pi}$ . Collision avoidance constraint is replaced by

$$\begin{cases} \|p_t - \hat{p}_{0:t}\|_2 \geq r + \hat{r} \\ \|p_t - \hat{p}_{1:t}\|_2 \geq r + \hat{r} \\ \dots \\ \|p_t - \hat{p}_{N-1:t}\|_2 \geq r + \hat{r} \end{cases} \quad \forall t \quad (6)$$

assuming that obstacles are in the same radius  $\hat{r}$ .  $\hat{p}_{N-1:t}$  denotes the position of  $N$ -th obstacle at the time step  $t$ . Kinematics of the robot is replaced by  $p_t = p_{t-1} + \Delta t \cdot \pi : (s_{0:t}, \{\hat{s}_{0:t}^{obs} \dots \hat{s}_{N-1:t}^{obs}\})$  where the historical states of all obstacles  $\{\hat{s}_{0:t}^{obs} \dots \hat{s}_{N-1:t}^{obs}\}$  are considered for generating the robot policy. Kinematics of the obstacles is replaced by

$$\begin{cases} \hat{p}_{0:t} = \hat{p}_{0:t-1} + \Delta t \cdot \hat{\pi} \\ \hat{p}_{1:t} = \hat{p}_{1:t-1} + \Delta t \cdot \hat{\pi} \\ \dots \\ \hat{p}_{N-1:t} = \hat{p}_{N-1:t-1} + \Delta t \cdot \hat{\pi} \end{cases} \quad (7)$$

### 2.3. Preliminary of RL and discrete soft actor critic

**Preliminary.** Markov decision process (MDP) is sequential decision process based on Markov Chain [36]. Markov Chain is defined by a variable set  $\mathbf{X} = \{X_n : n > 0\}$  where the probability  $p(X_{t+1} | X_t, \dots, X_1) = p(X_{t+1} | X_t)$ . This means the state and action of the next step only depend on the state and action of the current step. MDP is described as a tuple  $(S, A, P, R)$ .  $S$  denotes the state and here it refers to the state of robot and obstacles.  $A$  denotes an action taken by the robot. Action  $A = [\theta, v]$  is selected from *action space* where directions  $\theta \in \{0, \frac{\pi}{8}, \dots, 2\pi\}$  and Speed of each direction  $v \in \{0.2, 0.4, \dots, 1\}$ . Hence, action space consists of 81 actions including a stop action.  $P$  denotes the possibility to transit from one state to the next state.  $R$  denotes the reward or punishment received by the robot after executing actions. The reward function in this paper is defined by

$$R(s, a) = \begin{cases} 1 & \text{if } p_{current} = p_g \\ -0.1 + \frac{d_{min}}{2} & \text{if } 0 < d_{min} < 0.2 \\ -0.25 & \text{if } d_{min} < 0 \\ \frac{d_{start\_to\_goal} - (p_g - p_{current})}{d_{start\_to\_goal}} \cdot 0.5 & \text{if } t = t_{max} \text{ and} \\ 0 & \text{otherwise} \end{cases} \quad (8)$$

where  $p_{current}$  denotes the position of the robot currently.  $p_g$  denotes the position of the goal.  $d_{min}$  denotes the minimum distance of the robot and obstacles during motion planning process.  $d_{start\_to\_goal}$  denotes the distance of the start to the goal.  $t_{max}$  is the allowed maximum time for any episode of the motion planning. Our reward function (Eq. (8)) is modified from [18] which cannot work without the imitation learning. (Eq. (8)) accelerates convergence speed by attaching a reward to the *final position of the robot*. This encourages the robot to approach the goal.

Other crucial terms of RL include the *value*, *policy*, *value function*, and *policy function*. Value denotes *how good one state is or how good one action is in one state*. The value consists of the *state value* ( $V$  value) and *state-action value* ( $Q$  value). Value is defined by the expectation of accumulative rewards  $V(s) = \mathbb{E}[R_{t+1} + \gamma R_{t+2} + \dots + \gamma^{T-1} R_T | s_t]$  or  $Q(s, a) = \mathbb{E}[R_{t+1} + \gamma R_{t+2} + \dots + \gamma^{T-1} R_T | (s_t, a_t)]$  where  $\gamma$  is a discounted factor. The policy denotes the way to select actions. In function approximation case, policy is represented by the neural network. Value function in deep RL scope is represented by neural networks to estimate the value of environmental state via the function approximation [37]. Policy function is also represented by neural networks. Actions are selected by indirect way (e.g.,  $a \leftarrow \text{argmax}_a R(s, a) + Q(s, a; \theta)$  in DQN [13, 38]) or direct way (e.g.,  $\pi_\theta : s \rightarrow a$  in the actor-critic algorithm [39]).

**Discrete soft actor critic.** The policy of classical RL algorithm is obtained by maximizing the objective  $\sum_{t=0}^T \mathbb{E}_{(s_t, a_t) \sim \rho_\pi} [r(s_t, a_t)]$ . The objective of SAC is defined by the maximum entropy objective that considers the reward and entropy simultaneously

$$J(\pi) = \sum_{t=0}^T \mathbb{E}_{(s_t, a_t) \sim \rho_\pi} [r(s_t, a_t) + \alpha \mathcal{H}(\pi(\cdot | s_t))], \quad \mathcal{H}(\pi(\cdot | s_t)) = -\log \pi(\cdot | s_t) \quad (9)$$

where  $\mathcal{H}(\pi(\cdot | s_t))$  denotes the entropy.  $\alpha$  is the temperature parameter. In objective maximization, SAC policy converges to optimal policy certainly by the soft policy iteration which consists of *policy evaluation* and *policy improvement*. Optimal policy is obtained by repeated

application of policy evaluation and policy improvement. Policy evaluation [28] proves that if  $Q^{k+1} = \mathcal{T}^\pi(Q^k)$ ,  $Q^k$  will converge to the soft Q value of  $\pi$  when  $k \rightarrow \infty$ .  $\mathcal{T}^\pi(\cdot)$  is a modified Bellman backup operator given by

$$\mathcal{T}^\pi(Q)(s_t, a_t) \triangleq r(s_t, a_t) + \gamma \mathbb{E}_{s_{t+1} \sim p} [V(s_{t+1})] \quad (10)$$

where

$$V(s_t) = \mathbb{E}_{a_t \sim \pi} [Q(s_t, a_t) - \log \pi(a_t | s_t)]. \quad (11)$$

Applying  $\mathcal{T}^\pi(\cdot)$  to Q value will bring Q value closer to  $Q^\pi$ . This means  $Q(s_t, a_t) \leq \mathcal{T}^\pi(Q)(s_t, a_t) \leq Q^\pi(s_t, a_t)$ . Policy improvement [28] proves that  $Q^{\pi_{new}} \geq Q^{\pi_{old}}$  in objective maximization.  $\pi_{new}$  is defined by

$$\pi_{new} = \underset{\pi' \in \Pi}{\operatorname{argmin}} D_{KL} \left( \pi'(\cdot | s_t) \parallel \frac{\exp(Q^{\pi_{old}}(s_t, \cdot))}{Z^{\pi_{old}}(s_t)} \right) \quad (12)$$

where  $Z^{\pi_{old}}(s_t)$  is the partition function for distribution normalization. It can be ignored because it does not contribute to the gradient of new policy.  $Q^{\pi_{old}}$  guides the policy update to ensure an improved new policy. New policy is constrained to a parameterized family of distribution  $\pi' \in \Pi$  like Gaussians to ensure the tractable and optimal new policy. Given the repeated application of policy evaluation and improvement, policy  $\pi$  eventually converges to optimal policy  $\pi^*$ ,  $Q^{\pi^*} \geq Q^\pi, \pi \in \Pi$ .

SAC is the combination of *soft policy iteration* and *function approximation*. In (Eq. (9)), temperature  $\alpha$  is either a fixed value or an adaptive value. In function approximation, networks  $\theta$ , and  $\phi$  are used to approximate the action value and policy value. The action value objective and its gradient are obtained by

$$\begin{cases} J(\theta) = \mathbb{E}_{(s_t, a_t) \sim \mathcal{D}} \left[ \frac{1}{2} (Q(s_t, a_t; \theta) - \bar{Q}(s_t, a_t))^2 \right] \\ \bar{Q}(s_t, a_t) = r(s_t, a_t) + \gamma \mathbb{E}_{s_{t+1} \sim p} [V(s_{t+1}; \bar{\theta})] \\ \nabla_\theta J(\theta) \\ = \nabla_\theta Q(s_t, a_t; \theta) \cdot (Q(s_t, a_t; \theta) - r(s_t, a_t) + \gamma V(s_{t+1}; \bar{\theta}) - \alpha \log \pi_\phi(a_{t+1} | s_{t+1})) \end{cases} \quad (13)$$

where state value is approximated by  $V(s_{t+1}; \bar{\theta})$ .  $\bar{\theta}$  is the target action value network.  $\gamma$  is a discount factor. The policy objective and its gradient are obtained by

$$\begin{cases} J(\phi) = \mathbb{E}_{s_t \sim \mathcal{D}} \left[ D_{KL} \left( \pi_\phi(\cdot | s_t) \parallel \frac{\exp(Q(s_t; \theta))}{Z_\theta(s_t)} \right) \right] \\ = \mathbb{E}_{s_t \sim \mathcal{D}} \left[ \mathbb{E}_{a_t \sim \pi_\phi} [\alpha \log \pi_\phi(a_t | s_t) - Q(s_t, a_t; \theta)] \right] \\ \nabla_\phi J(\phi) = \nabla_\phi \alpha \log \pi_\phi(a_t | s_t) + \\ \nabla_\phi f_\phi(\epsilon_t; s_t) \cdot (\nabla_{a_t} \alpha \log \pi_\phi(a_t | s_t) - \nabla_{a_t} Q(s_t, a_t)) \\ a_t = f_\phi(\epsilon_t; s_t) \end{cases} \quad (14)$$

where  $f_\phi(\epsilon_t; s_t)$  is the network transformation.  $\epsilon_t$  is an input noise vector sampled from fixed distribution like spherical Gaussian. The temperature objective is defined by

$$J(\alpha) = \mathbb{E}_{a_t \sim \pi_t} [-\alpha \log \pi_t(a_t | s_t) - \alpha \bar{\mathcal{H}}] \quad (15)$$

where  $\bar{\mathcal{H}}$  is the target entropy. Temperature objective gradient is obtained by approximating dual gradient descent [40]. Eventually, the networks and temperature are updated by

$$\begin{cases} \theta \leftarrow \theta - \gamma_\theta \nabla_\theta J(\theta) \\ \phi \leftarrow \phi - \gamma_\phi \nabla_\phi J(\phi) \\ \alpha \leftarrow \alpha - \gamma_\alpha \nabla_\alpha J(\alpha) \\ \bar{\theta} \leftarrow \tau \theta + (1 - \tau) \bar{\theta} \end{cases} \quad (16)$$

SAC is used in tasks with continuous action space. However, the action space in this paper is discrete. Hence, SAC should be modified to

suit our task. Some modifications [29] should be made. They are summarized as the follows:

1) Q function should be moved from  $Q : S \times A \rightarrow \mathbb{R}$  to

$$Q : S \times A \rightarrow \mathbb{R}^{|A|}. \quad (17)$$

This means Q values of all possible actions should be outputted, instead of a Q value of the action taken by the robot.

2) The outputted policy should be the action distribution

$$\pi : S \rightarrow [0, 1]^{|A|} \quad (18)$$

instead of the *mean* and *covariance* of action distribution of SAC  $\pi : S \rightarrow \mathbb{R}^{2|A|}$ .

3) In temperature objective (Eq. (15)), its expectation  $\mathbb{E}_{a_t \sim \pi_t}[\cdot]$  is obtained by the Monte-Carlo estimation which involves taking an expectation over the action distribution [29]. In the discrete action space case, the expectation should be calculated directly, instead of Monte-Carlo estimation. Hence, the temperature objective changes into

$$J(\alpha) = \pi(s_t)^T [-\alpha \log \pi_t(s_t) - \alpha \bar{\mathcal{H}}] \quad (19)$$

Where  $\bar{\mathcal{H}}$  is the target entropy. Similarly, the policy objective changes into

$$J(\phi) = \mathbb{E}_{s_t \sim \mathcal{D}} [\pi(s_t)^T [\alpha \log \pi_\phi(s_t) - Q(s_t; \theta)]] \quad (20)$$

### 3. Method

This paper improves the robotic motion planning performance by improving SARL [18] where attention network and DQN are applied for environment interpretation and learning purposes respectively. To be specific, first, this paper improves the attention network for the environment interpretation by integrating the skip connection method and LSTM into the architecture of attention network. Second, DQN is replaced by DSAC which has not been used in motion planning tasks before. Thus, the network convergence is improved, and the training is stabilized.

In this section, we further present the implementation of RG-DSAC which works as one of baseline algorithms for comparisons. Then RG-DSAC is improved by introducing AW-DSAC which also works as one of baseline algorithms for comparisons. Finally, AW-DSAC is further improved by integrating the skip connection method and LSTM into the architecture of attention network of AW-DSAC, resulting in SA-DSAC and LSA-DSAC. An overview of mentioned four algorithms is shown in Fig. 3.

#### 3.1. Relation graph based DSAC (RG-DSAC)

The mechanism of relational graph [16] is shown in Fig. 3a. The source input collected from the environment consists of source robot feature  $s_r$  and  $N$ -obstacle features ( $o_i, i \in 1, 2, \dots, N$ ). These features are in different dimensions. They should be formatted to the same dimension to accommodate the input requirement of the graph by

$$s_{r\_emb-1} = MLP(s_r) \quad (21)$$

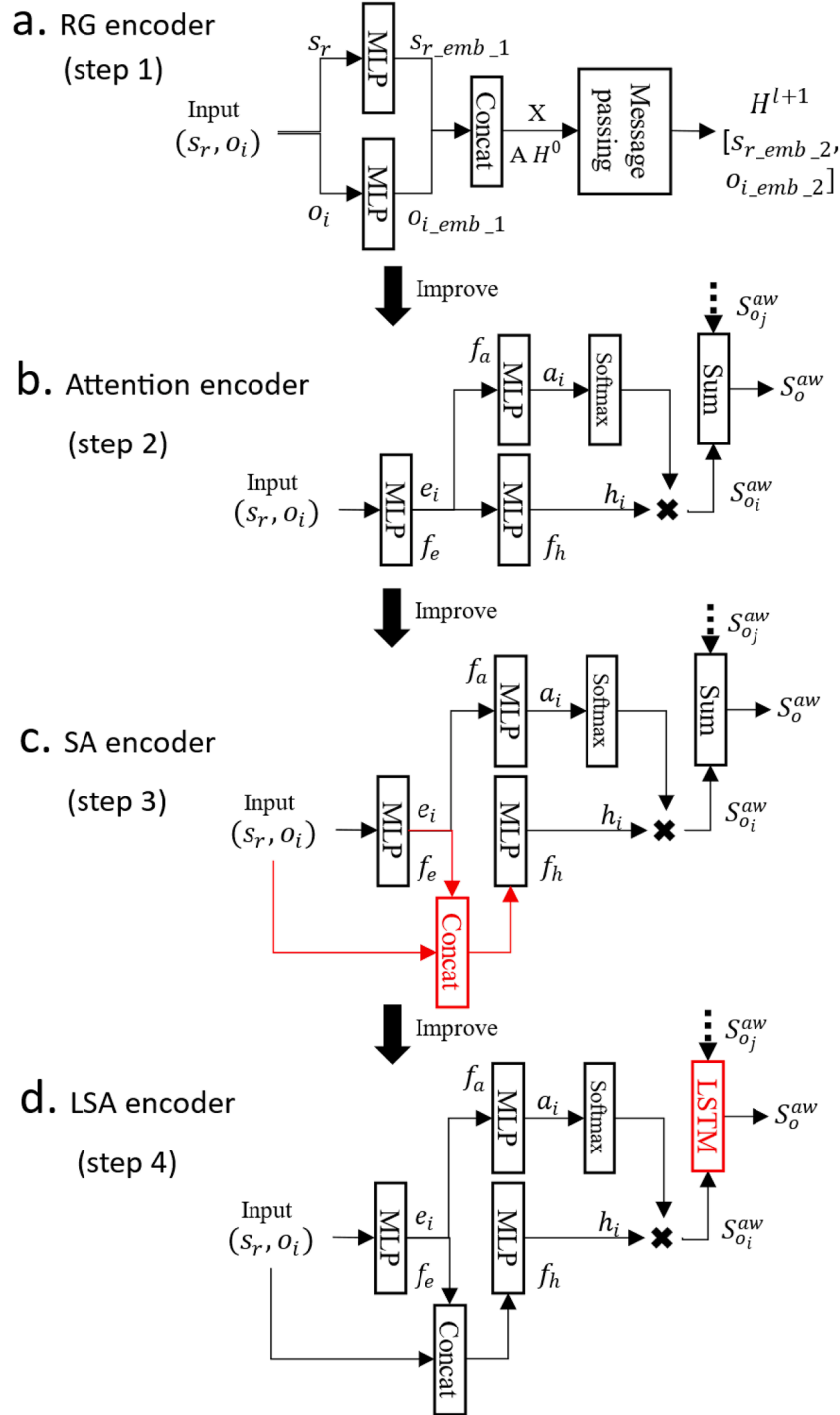


**Fig. 3.** Mechanisms of relational graph (a), attention network or attention weight (b), skip connection method for attention network (c), and LSTM and skip connection method for attention network (LSA) (d). In LSA encoder, the skip connection is for reducing the feature loss, while LSTM replaces the sum operator of the attention network to make the final interpreted features (environmental state) injective and stabilize the training. Note that here attention weigh is the weight of attention network. Attention weight can be used to generate attention score that makes the importance of obstacles interpretable.

$$O_{i\_emb\_1} = MLP(O_i) \quad (22)$$

They are achieved by the *multi-layer perceptron* (MLP).  $S_r\_emb\_1$  and  $O_{i\_emb\_1}$  denote the embeddings of the robot and  $i$ th obstacle feature. All obstacle features are concatenated to form the embedded obstacle state  $S_{o\_emb\_1}$ . The embedded robot state and embedded obstacle state are concatenated to form the initial feature matrix (environmental representation)  $X$  by

$$X = \text{concat}(S_r\_emb\_1, S_{o\_emb\_1}) \quad (23)$$

The first row of  $X$  ( $X[0, :]$ ) denotes the robot feature and remaining rows ( $X[i, :], i \in 1, 2, \dots, N$ ) denotes all obstacle features.

Given feature matrix  $X$ , relation matrix  $A$  that represents the relationship of the *robot-obstacle* and *obstacle-obstacle* is computed by a *similarity function*. This is achieved by concatenating one of features in  $X[i, :], i \in 0, 1, \dots, N$  with all features in  $X[j, :], j \in 0, 1, \dots, N$  recursively to form the *pairwise features of the robot-obstacle and obstacle-obstacle*. Then,

the relation feature  $A[i, :]$  is obtained by MLP that maps these pairwise features to a fixed dimension (the same dimension as that of  $X[i, :]$ ) via

$$A[i, :] = \text{MLP}(\text{concat}(X[i, :], X[:, i])) \quad i \in 0, 1, \dots, N \quad (24)$$

Given feature matrix and relation matrix, interaction feature matrix  $H$  is obtained by the *message passing rule* from the *graph convolutional network* (GCN) via

$$H^{l+1} = \sigma(AH^lW^l) + H^l, \quad H^0 = H^1 = X, \quad l \in 0, 1, \dots \quad (25)$$

where  $\sigma$  is the activation function.  $W$  is layer-specific trainable weight, and  $l$  denotes the number of the neural network layers. The *difference* between the initial feature matrix  $X$  and the interaction feature matrix  $H$  is that  $H$  includes both initial features and relation features, while  $X$  only includes initial features. Interaction feature matrix  $H^{l+1}$  outperforms initial feature matrix  $X$  in the *expressive power*. This is achieved via the relation matrix  $A$  and the message passing, and it is shown by training and evaluation performances in the simulation and real-world motion planning. Moreover, the expressive power of the interaction feature can be further improved by LSTM that maps interaction feature of obstacles  $H^{l+1}[1, :]$  to the sequential hidden features. Hence, final output of the relational graph (environmental state) that feeds DSAC consists of interaction feature of the robot and obtained sequential hidden features via

$$S^g = [H^{l+1}[0, :], \text{LSTM}(H^{l+1}[1, :])] \quad (26)$$

### 3.2. Attention weight based DSAC (AW-DSAC)

Given the relational graph, it is obvious that relation matrix  $A$  plays an essential role to improve the expressive power of output features. Relation matrix includes the robot-obstacle relation and obstacle-obstacle relation. Now, let's recall our task: robotic motion planning among dense obstacles. It is easy to see that robot-obstacle relation matters in our task. However, obstacle-obstacle relation does not show much *direct importance* in this task to generate features with high expressive power, although it has *marginal importance* to predict future obstacle trajectories that slightly improve the motion planning performance [16]. To further improve the motion planning performance, much attention should be paid to making the best of the robot-obstacle relation. Moreover, the importance of the obstacles also vary in different time step. The importance is shown by the robot speed, moving directions, and distance of robot and obstacle.

Recent attention weight mechanism [18] focuses on the pairwise robot-obstacle feature. It computes an attention score that weighs the importance of dynamic obstacles and makes the expressive power of interpreted environmental state interpretable. Hence, we apply the attention weight to replace relational graph for high and interpretable expressive power of the output features.

As the relational graph, in the attention weight case (Fig. 3b), the environmental state to feed DSAC  $S^{aw}$  is defined by the feature combination of the robot and obstacles via

$$S^{aw} = [s_r, S_o^{aw}] \quad (27)$$

where  $S_o^{aw}$  denotes the weighted obstacle feature, and it is defined by

$$S_o^{aw} = \sum_{i=1}^n [\text{softmax}(\alpha_i)] \cdot h_i \quad (28)$$

where  $\alpha_i$  and  $h_i$  denote the *attention score* and the *interaction feature* of the robot and the obstacle  $o_i$  respectively. The interaction feature is a high-level feature that better outlines a robot-obstacle relation, compared to a shallow feature  $e_i$ . The interaction feature is defined by

$$h_i = f_h(e_i; w_h) \quad (29)$$

where  $f_h(\cdot)$  and  $w_h$  denote the MLP and its weight.  $e_i$  denotes the *embedded shallow feature* obtained from the pairwise robot-obstacle feature  $[s_r, o_i]$ . The attention score is defined by

$$\alpha_i = f_a(e_i; w_a) \quad (30)$$

where  $f_a(\cdot)$  and  $w_a$  denote the MLP and its weight. The embedded shallow feature is defined by

$$e_i = f_e([s_r, o_i]; w_e), \quad i \in 1, 2, \dots, N \quad (31)$$

where  $f_e(\cdot)$  and  $w_e$  denote the MLP and its weight.

### 3.3. Skip connection for attention weight based DSAC (SA-DSAC)

Recent progress in supervised DL [41–43] unveils that low-level (shallow) and high-level (deep) features play different role in the learning of the neural networks. The low-level feature provides more details of the source environmental state, while high-level feature outlines an overall structure of source environmental feature. Both low-level and high-level features contribute to the expressive power. Obviously, the attention weight mechanism just includes high-level feature to form the interaction feature  $h_i$ , given the mechanism of the attention weight in Fig. 3b. This causes the loss of the details in environmental state and low expressive power of final feature  $S^{aw}$  follows. To improve the expressive power of environmental state interpreted by attention weight, we introduce SA-DSAC that integrates the skip connection method (Fig. 3c) into the architecture of the attention network for generating optimized interaction feature by

$$h_i = f_h(\text{concat}(e_i, [s_r, o_i]); w_h) \quad (32)$$

where  $f_h(\cdot)$  and  $w_h$  denote the MLP and its weight.  $e_i$  denotes the *embedded shallow feature* obtained from the pairwise robot-obstacle feature  $[s_r, o_i]$ .

### 3.4. LSTM and skip connection for attention weight based DSAC (LSA-DSAC)

Given the attention weight mechanism, we can notice that weighted obstacle features  $S_o^{aw}$  are pooled by summing all weighted interaction features. Recent research [44] unveils a high performance of the sum operation over the *mean* and *max* operations in pooling features for generating new features with high expressive power. However, it does not mean that sum operation is absolute *injective* [44] and robust to the unstable training (e.g., vanishing gradient) in the case with deep networks. The more injective the feature is, the more distinguishable the feature is against other features. Hence, high injectivity of feature means high expressive power [44]. Sum operation just outlines an overall structure of pooled features, and some pooled features based on the sum operation lack injectivity or are undistinguishable. For instance, *sum* (3, 1) and *sum* (2, 2). Features [3, 1] and [2, 2] are equal statistically, but they are obviously different features. We think that *keeping some source features in the feature pooling process* contributes to the injectivity of pooled features. Moreover, with the networks because complex and deeper, sum operation is not robust enough to the vanishing gradient. This may result in unstable training and consequent divergence.

LSTM is expected to be a good solution to achieve this goal where the source features are just mapped into sequential hidden features. In this process, the structural information, and a part of the feature details of the source features are kept, instead of just keeping the statistical property of source features via the sum operation. Additionally, when networks become deeper, LSTM helps stabilize the gradient due to its activation function (identity function). This avoids the case where small gradient becomes zero with the training. Hence, we introduce LSA-DSAC that takes LSTM to replace sum operation in the pooling of weighted obstacle feature  $S_o^{aw}$ . LSTM maps weighted interaction features

$\text{softmax}(\alpha_i) \cdot h_i$  to sequential features (Fig. 3d). This better preserves the feature of each weighted interaction feature and avoids potential vanishing gradient in the case of deep networks. This is achieved by

$$S_o^{aw} = \text{LSTM}[\text{softmax}(\alpha_i) \cdot h_i], \quad i \in 1, 2, \dots, N \quad (33)$$

**Mechanism of LSA-DSAC.** Overall, the mechanism of LSA-DSAC consists of two components/steps: 1) LSA encoder (Fig. 3d) that is optimized from attention network. 2) the combination of LSA encoder and DSAC. The LSA encoder processes the source environment state to prepare environment encoding/embedding for original policy network of DSAC (that are MLPs), thus the policy (new policy network) is prepared. The critic (new critic network) is also prepared as the same way (Fig. 4a). Then, the policy and critic are updated in the backpropagation process (Fig. 4b). Specifically, once the environmental state  $S_o^{aw} = [s_r, S_o^{aw}]$  generated by LSA is well prepared, it will feed DSAC to generate trained models for the motion planning of the robot. The attention network connects with the prediction network (original policy/critic network of DSAC) to form the new critic or policy (Fig. 4a and Algorithm 1). In implementation, separate attention networks are taken to form the critic and policy of DSAC by

$$\text{critic} = [\theta_{att_c}, \theta_{c1}, \theta_{c2}] \quad (34)$$

$$\text{policy} = [\theta_{att_p}, \theta_p] \quad (35)$$

where double Q-network architecture (networks  $\theta_{c1}, \theta_{c2}$ ) is taken in critic to reduce the overestimation of the Q value, while policy just has single network  $\theta_p$  for prediction.

The training process of LSA-DSAC is shown in Fig. 4b. Episodic data  $\langle s, a, r, s' \rangle$  of each time step is obtained by performing the policy of DSAC

$$\langle s_t, a_t, r_t, s_{t+1} \rangle \sim \pi(a_t | s_t; [\theta_{att_p}, \theta_p]) \quad (36)$$

Episodic data  $\mathcal{E}$  is stored in replay buffer  $\mathcal{D}$  at the end of each episode by

$$\mathcal{D} \leftarrow \mathcal{D} \cup \mathcal{E}, \quad \mathcal{E} = \mathcal{E} + \langle s_t, a_t, r_t, s_{t+1} \rangle \quad (37)$$

where experience in each step  $\langle s_t, a_t, r_t, s_{t+1} \rangle$  is attached to historical experience to update the episodic data.

Networks are trained in each step of an episode (Algorithm 2). In the forward propagation process, the critic loss  $\mathcal{L}_{loss_Q}$  and policy loss  $\mathcal{L}_{loss_P}$  are obtained by

$$\mathcal{L}_{loss_Q} = \text{MSE}(Q(a|s)_{c1}, Q_{next\_dis}) + \text{MSE}(Q(a|s)_{c2}, Q_{next\_dis}) \quad (38)$$

$$\mathcal{L}_{loss_P} = -\text{mean}[\mathbb{E}_{s \sim p}[Q(s)] + \alpha \cdot \mathcal{H}(\pi(\cdot|s))] \quad (39)$$

where  $Q_{next\_dis}$  and  $Q(a|s)_{ci}, i \in \{1, 2\}$  denote the discounted next state value and current action values respectively.  $\mathbb{E}_{s \sim p}[Q(s)]$  and  $\mathcal{H}(\pi(\cdot|s))$  denote the expectation of current state value and current policy entropy

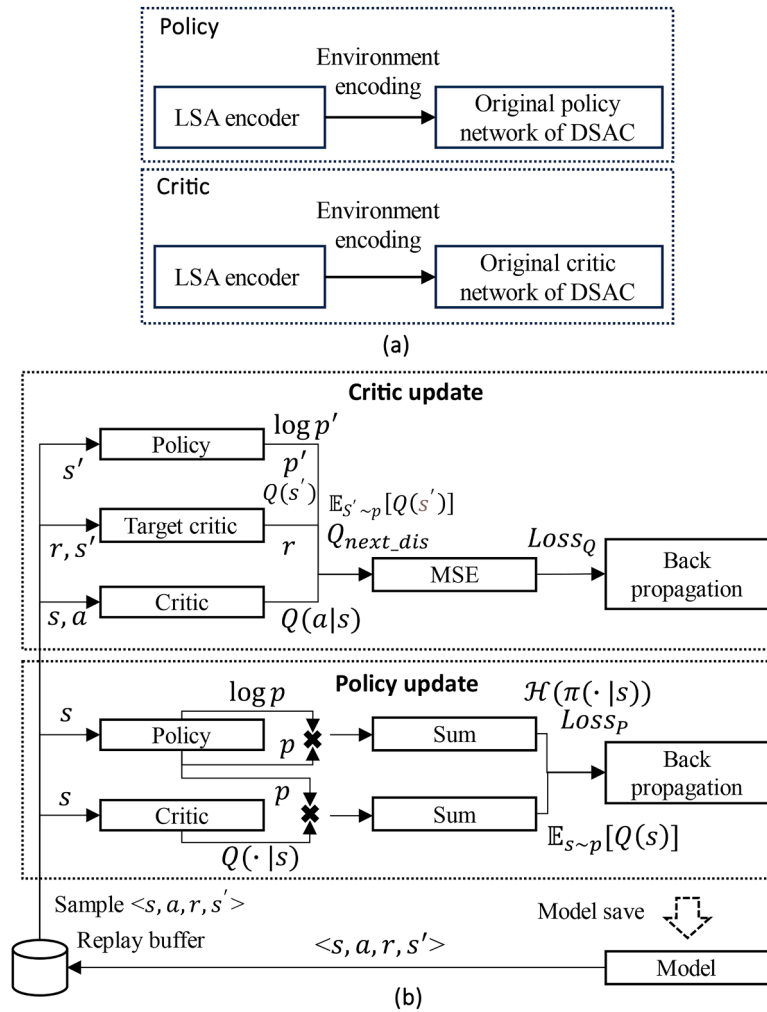


**Fig. 4.** Mechanism and training process of our LSA-DSAC. LSA-DSAC starts by collecting data from the environment using the initialized models. Collected data is saved in the replay buffer from which data is sampled. The policy and critic are updated based on sampled data until convergence, resulting in trained models which are saved for evaluations in the motion planning tasks.

**Algorithm 1**  
 LSA-DSAC.

---

```

1. Initialize the replay buffer  $\mathcal{D}$ 
2. Initialize attention net of critic  $\theta_{att-c}$ , attention net of policy  $\theta_{att-p}$ , prediction nets
   of critic  $\theta_{c1}$  and  $\theta_{c2}$ , and prediction net of policy  $\theta_p$  where
    $critic = [\theta_{att-c}, \theta_{c1}, \theta_{c2}]$ ,  $policy = [\theta_{att-p}, \theta_p]$ 
3. Initialize target critic  $[\bar{\theta}_{att-c}, \bar{\theta}_{c1}, \bar{\theta}_{c2}]$ :
    $\bar{\theta}_{att-c} \leftarrow \theta_{att-c}$ ,  $\bar{\theta}_{c1} \leftarrow \theta_{c1}$ ,  $\bar{\theta}_{c2} \leftarrow \theta_{c2}$ 
4. For episode  $i < N$  do
5.   For  $t \neq T_{terminal}$  in episode  $i$  do
6.     Execute action:
        $\langle s_t, a_t, r_t, s_{t+1} \rangle \sim \pi(a_t | s_t; [\theta_{att-p}, \theta_p])$ 
7.     Train If length  $(\mathcal{D}) <$  batch size  $l$ 
8.     Store data of this episode:
        $\mathcal{E} = \mathcal{E} + \langle s_t, a_t, r_t, s_{t+1} \rangle$ 
9.     Update replay buffer:  $\mathcal{D} \leftarrow \mathcal{D} \cup \mathcal{E}$ 
10.     $i = i + 1$ 
11.   Save models:  $\theta_{att-c}$ ,  $\theta_{att-p}$ ,  $\theta_{c1}$ ,  $\theta_{c2}$  and  $\theta_p$ 

```

---

respectively.  $\alpha$  denotes the temperature parameter. These intermediate values including  $Q_{next-dis}$ ,  $Q(a|s)_{ci}$ ,  $i \in \{1, 2\}$ ,  $\mathbb{E}_{s \sim p}[Q(s)]$ , and  $\mathcal{H}(\pi(\cdot|s))$  are computed as the follows:

**Compute discounted next state value.**  $Q_{next-dis}$  is computed by

$$Q_{next-dis} = r(s, a) + \gamma \mathbb{E}_{s' \sim p}[Q(s')] \quad (40)$$

**Algorithm 2**  
 Train.

---

```

1. Sample  $K$ -batch experiences randomly from replay buffer  $\mathcal{D}$ 
   //Prepare discounted next state value  $Q_{next-dis}$ 
2. Compute next policy distribution  $p'$  and its logit value  $\log p'$ :
   Forward-propagation-policy
3. Compute next state value  $Q(s')_{c1}$ ,  $Q(s')_{c2}$  by target critic:
   Forward-propagation-critic
4. Compute expectation of next state value:
    $\mathbb{E}_{s' \sim p}[Q(s')] = \sum [p' \cdot \min(Q(s')_{c1}, Q(s')_{c2}) - \alpha \cdot \log p']$ 
5. Compute discounted next state value:
    $Q_{next-dis} = r(s, a) + \gamma \mathbb{E}_{s' \sim p}[Q(s')]$ 
   //Prepare current action value  $Q(a|s)_{c1}$ ,  $Q(a|s)_{c2}$ 
6. Compute current state value  $Q(s)_{c1}$ ,  $Q(s)_{c2}$ :
   Forward-propagation-critic
7. Compute current action value  $Q(a|s)_{c1}$ ,  $Q(a|s)_{c2}$ :
    $Q(a|s)_{c1} = Q(s)_{c1} \cdot gather(a)$ 
    $Q(a|s)_{c2} = Q(s)_{c2} \cdot gather(a)$ 
   //Prepare Q value loss (critic loss)
8. Compute Q value loss:
    $\mathcal{L}_{ossQ} = MSE(Q(a|s)_{c1}, Q_{next-dis}) + MSE(Q(a|s)_{c2}, Q_{next-dis})$ 
   //Prepare policy entropy
9. Compute policy distribution  $p$  and its logit value  $\log p$ :
   Forward-propagation-policy
10. Compute current policy entropy:
    $\mathcal{H}(\pi(\cdot|s)) = -\log \pi(\cdot|s) = -\sum p \cdot \log p$ 
   //Prepare expectation of current state value
11. Compute current state value  $Q(\cdot|s)_{c1}$ ,  $Q(\cdot|s)_{c2}$  for all actions where  $Q(\cdot|s) = Q(s)$ :
   Forward-propagation-critic
12. Compute expectation of current state value:
    $\mathbb{E}_{s \sim p}[Q(s)] = \sum \min[(Q(s)_{c1}, Q(s)_{c2}) \cdot p]$ 
   //Prepare policy and temperature loss
13. Compute policy loss:
    $\mathcal{L}_{ossP} = -\text{mean}[\mathbb{E}_{s \sim p}[Q(s)] + \alpha \cdot \mathcal{H}(\pi(\cdot|s))]$ 
14. Compute temperature loss:
    $\mathcal{L}_\alpha = -\min[\log \alpha \cdot (\bar{\mathcal{H}} - \mathcal{H})]$ 
   //Back-propagation to update networks and temperature
15. Update attention net  $\theta_{att-c}$  and prediction nets of critic  $\theta_{c1}$  and  $\theta_{c2}$ :
    $\theta_{att-c, ci} \leftarrow \theta_{att-c, ci} - \gamma \nabla_{\theta_{att-c, ci}} \mathcal{L}_{ossQ}$ ,  $i \in \{1, 2\}$ 
16. Update attention net  $\theta_{att-p}$  and prediction nets of policy  $\theta_p$ :
    $\theta_{att-p, p} \leftarrow \theta_{att-p, p} - \gamma \nabla_{\theta_{att-p, p}} \mathcal{L}_{ossP}$ 
17. Update temperature:
    $\alpha \leftarrow \alpha - \gamma \nabla_\alpha \mathcal{L}_\alpha$ ,  $\alpha \leftarrow e^\alpha$ 
18. Update target critic  $[\bar{\theta}_{att-c}, \bar{\theta}_{c1}, \bar{\theta}_{c2}]$ :
    $\bar{\theta}_{att-c} \leftarrow \theta_{att-c}$ ,  $\bar{\theta}_{c1} \leftarrow \theta_{c1}$ ,  $\bar{\theta}_{c2} \leftarrow \theta_{c2}$ 

```

---

where  $r(s, a)$  denotes the reward from the environment after executing action  $a$  in state  $s$ .  $\mathbb{E}_{s' \sim p}[Q(s')]$  denotes the expectation of the next state value.  $\gamma$  denotes a discount factor.  $\mathbb{E}_{s \sim p}[Q(s)]$  is computed by

$$\mathbb{E}_{s \sim p}[Q(s)] = \sum [p' \cdot \min(Q(s')_{c1}, Q(s')_{c2}) - \alpha \cdot \log p'] \quad (41)$$

where  $Q(s')_{c1}$  and  $Q(s')_{c2}$  denote the next state values computed by the target critic via the algorithm *Forward-propagation-critic*.  $p'$  and  $\log p'$  denote the next policy distribution and its logit value. They are computed by *Forward-propagation-policy*.

The forward propagations of the critic and policy (Algorithms 3 and 4) are almost the same. Their difference is that the critic takes two networks to compute two Q values by

$$Q(s)_{c1}, Q(s)_{c2} \leftarrow f_{\theta_{ci}}(S^{aw}), i \in \{1, 2\} \quad (42)$$

Then, an average Q value is obtained. This reduces the bias (over-estimation) of the Q value. The policy just takes single network to compute policy distribution and its logit value by

$$\log p, p \leftarrow f_{\theta_p}(S^{aw}) \quad (43)$$

**Compute current action values.** To obtain  $Q(a|s)_{ci}$ ,  $i \in \{1, 2\}$ , current state values  $Q(s)_{ci}$ ,  $i \in \{1, 2\}$  should be computed first by the algorithm *Forward-propagation-critic*. Then, current action values are computed by gathering state value along the policy distribution of the action  $a$  via

$$Q(a|s)_{c1} = Q(s)_{c1} \cdot gather(a), Q(a|s)_{c2} = Q(s)_{c2} \cdot gather(a) \quad (44)$$

**Compute expectation of current state value.** The process to compute the expectation of current state value is different from that of the next state value. It is computed by

$$\mathbb{E}_{s \sim p}[Q(s)] = \sum \min[(Q(s)_{c1}, Q(s)_{c2}) \cdot p] \quad (45)$$

where  $Q(s)_{ci}$ ,  $i \in \{1, 2\}$  and  $p$  are computed respectively by *Forward-propagation-critic* and *Forward-propagation-policy*.

**Compute policy entropy.**  $\mathcal{H}(\pi(\cdot|s))$  is computed by

$$\mathcal{H}(\pi(\cdot|s)) = -\log \pi(\cdot|s) = -\sum p \cdot \log p \quad (46)$$

Before the back-propagation process, the temperature loss  $\mathcal{L}_\alpha$  is also required for the network update.  $\mathcal{L}_\alpha$  is computed by

$$\mathcal{L}_\alpha = -\min[\log \alpha \cdot (\bar{\mathcal{H}} - \mathcal{H})] \quad (47)$$

where  $\bar{\mathcal{H}}$  is the target entropy. Then, the temperature and all networks are updated by the gradient ascent via

$$\theta_{att-c, ci} \leftarrow \theta_{att-c, ci} - \gamma \nabla_{\theta_{att-c, ci}} \mathcal{L}_{ossQ}, i \in \{1, 2\} \quad (48)$$

$$\theta_{att-p, p} \leftarrow \theta_{att-p, p} - \gamma \nabla_{\theta_{att-p, p}} \mathcal{L}_{ossP} \quad (49)$$

$$\alpha \leftarrow \alpha - \gamma \nabla_\alpha \mathcal{L}_\alpha, \alpha \leftarrow e^\alpha \quad (50)$$

Finally, target critic is also updated for a new training round via

$$\bar{\theta}_{att-c} \leftarrow \theta_{att-c}, \bar{\theta}_{c1} \leftarrow \theta_{c1}, \bar{\theta}_{c2} \leftarrow \theta_{c2} \quad (51)$$

## 4. Experiments

This section presents the implementation details of our algorithms. First, the network framework of our LSA-DSAC is given. Second, the model training details of our algorithms and the state-of-the-art are presented. Third, the model evaluations are conducted. The evaluations include the converged reward evaluation, interpretability evaluation, qualitative evaluation, quantitative evaluation, time complexity evaluation, transferability evaluation, and robustness evaluation. Finally, the physical implementation is presented. Note that our LSA-DSAC and other algorithms for comparisons share the same input, which is the

features of the robot and obstacles. Main hardware is Intel Core i7-9750H processor with 16-GB memory. The trainings and evaluations are based on the CrowdNav simulation system [18].

#### 4.1. Network framework

In implementation, the network framework of our LSA-DSAC (Fig. 5) takes the architecture with separate attention networks. The prediction networks of the critic and policy connect with different attention network to form the critic and policy of DSAC. This contributes to overall convergence, compared with architecture with a shared attention network. The prediction network of the critic consists of two linear networks. Each linear network has three linear layers. The prediction network of the policy just has one linear network that also has three linear layers.

#### 4.2. Model training

We first implemented RG-DSAC for motion planning in the circle-crossing simulator. The training result (Fig. 6a) demonstrated that RG-DSAC converged faster than DSAC with source environmental state. Moreover, the converged result of RG-DSAC also outperformed the DSAC with source environmental state.

The output of the relational graph is the matrix  $H^{l+1}$  (layer number  $l = 2$ ). The final interpreted feature to feed DSAC  $S^{\mathcal{R}}$  is the combination of the robot feature  $H^{l+1}[0, :]$  and the pooled obstacle features  $LSTM(H^{l+1}[1 :, :])$  where obstacle features are pooled by LSTM. To prove the efficacy and efficiency of our method to prepare the final features for training ( $rob+lstm(obs)$ ), we compared it with other potential features for training by the ablation experiments where other features include:

- 1) features based on the feature concatenation of the robot and obstacles ( $rob+obs$ ),
- 2) source robot feature ( $rob$ ),
- 3) features from summing concatenated feature of the robot and obstacle ( $sum(rob+obs)$ ),
- 4) features from concatenating the robot feature and obstacle features pooled by MLP ( $rob+mlp(obs)$ ),
- 5) pooled features of the robot and obstacles by MLP ( $mlp(rob+obs)$ ), and
- 6) pooled features of the robot and obstacles by LSTM ( $lstm(rob+obs)$ ).

Ablation experiments (Fig. 6b) demonstrate that interpreted features for training using our method outperforms other potential features. Experiments also indicate that the robot feature should be separated from the obstacle features pooled by LSTM or MLP, resulting in the features  $rob+lstm(obs)$  and  $rob+mlp(obs)$ . This contributes to the expressive power of interpreted features for training. The interpreted feature  $rob+mlp(obs)$  marginally contributes to the convergence, while the interpreted feature  $rob+lstm(obs)$  by our LSA-DSAC dramatically

#### Algorithm 3

Forward-propagation-critic.

---

```

//Prepare input to feed prediction nets  $\theta_{ci}, i \in \{1, 2\}$ 
1. Calculate embedded shallow feature:
 $e_i = f_e(s; w_e), i \in 1, 2, \dots, N$ 
2. Calculate optimized interaction feature:
 $h_i = f_h(\text{concat}(e_i, [s_r, o_i]); w_h)$ 
3. Calculate attention score and its softmax value:
 $\alpha_i = f_a(e_i; w_a)$ 
4. Calculate weighted feature of each obstacle:
 $[\text{softmax}(\alpha_i)] \cdot h_i, i \in 1, 2, \dots, N$ 
5. Pool weighted feature of obstacles by LSTM:
 $S_o^{sw} = LSTM[\text{softmax}(\alpha_i) \cdot h_i], i \in 1, 2, \dots, N$ 
6. Obtain input data  $S^{sw}$  for prediction net:  $S^{sw} = [s_r, S_o^{sw}]$ 
//Prepare state value of  $\theta_{c1}$  and  $\theta_{c2}$ 
7. Calculate state values:  $Q(s)_{c1}, Q(s)_{c2} \leftarrow f_{\theta_{ci}}(S^{sw})$ 

```

---

improves the convergence.

We noticed that a separate architecture (two relation networks and two LSTM) outperforms a shared architecture (one shared relation network with shared and separate LSTMs) (Fig. 6c) in the implementation of RG-DSAC. Experiment shows that separate LSTM encoding contributes to the convergence dramatically (yellow and green curves), while a separate relation network also contributes to the convergence (blue and yellow curves).

In Fig. 6d, the convergence is improved after the attention network replaces the relational graph for the feature interpretation. Then, the convergence is further improved by integrating the skip connection method and LSTM to the attention network. Experiment also shows that AW-DSAC and SA-DSAC are unstable in training because of the sum operation that lacks robustness to vanishing gradient and injectivity. LSA-DSAC outperforms the rest algorithms in converged result by sacrificing the convergence speed at early-stage training. The experiment is extended to 10-obstacle cases (Fig. 6e) where our LSA-DSAC still outperforms the rest algorithms in overall convergence speed and converged result. LSA-DSAC is also trained in cases with 1, 2, 3 and 4 obstacles (Fig. 6f). The experiment shows that the increase of the environmental complexity (the number of dynamic obstacles) results in a decrease of convergence.

Finally, LSA-DSAC is compared with RG-DSAC and the state-of-the-art that includes CADRL, LSTM-A2C, LSTM-RL and SARL. Note that ORCA is not trainable and it is not included in the training comparisons. LSA-DSAC is compared with CADRL in 1-obstacle case because CADRL only supports single-obstacle training (Fig. 6g). The rest state-of-the-art supports multi-obstacle training and they are trained in cases with 5 and 10 obstacles (Fig. 6h-i). Experiment shows that our LSA-DSAC is superior to the state-of-the-art in both convergence speed and converged result. The training parameters of our LSA-DSAC is shown in Table 1.

#### 4.3. Model evaluation

Trained models of all algorithms are evaluated in 5-obstacle case comprehensively in the circle-crossing simulator from seven perspectives. This includes the converged reward evaluation, interpretability (explainable ability) evaluation, qualitative evaluation, quantitative evaluation, time complexity evaluation, transferability evaluation, and robustness evaluation. Models are evaluated with 500 test sets (episodes).

**Converged reward evaluation.** Converged reward indicates the overall performance of the trained models in small test set during training. It provides a fast impression about how good the model is in training. It is easy to see that our LSA-DSAC outperforms the state-of-the-art in the converged reward, while SARL performs best among the state-of-the-art (Table 2). CADRL just supports training with one obstacle, therefore its model is not included in comparison.

**Interpretability (explainable ability) evaluation.** Interpretability (explainable ability) here is defined as the ability to decide directly, explicitly, and uniformly how good the motion planning performance is. Attention mechanism (attention network) provides the attention score (a post-training indicator) to evaluate the importance of obstacles, therefore justifying the robot's policy or actions. Then, motion planning strategy is generated based on the attention score. Motion planning strategy (Fig. 7) of our LSA-DSAC indicates that the attention score is an overall evaluation that considers the moving direction, moving speed, and distance of robot and obstacles (e.g., humans). The distance of robot and obstacles sometimes contributes less to the attention score (e.g., human 2 in Fig. 7 that has minimum distance to the robot). Interpretability comparisons of the models are shown in Table 3. Our LSA-DSAC and SARL have interpretability because of the attention score, while the motion planning performance of the rest algorithms cannot be observed indirectly, explicitly, and unexplainably.

**Qualitative evaluation.** The quality here refers to the trajectory quality of the robot in an episode. In 500 tests, the robot based on our algorithms and state-of-the-art (trainable) learnt some of the six motion

**Algorithm 4**

Forward-propagation-policy.

---

```

//Prepare input to feed prediction net  $\theta_p$ 
1. Calculate shallow feature:  $e_i = f_e(s; w_e), i \in 1, 2, \dots, N$ 
2. Calculate optimized interaction feature:
    $h_i = f_h(\text{concat}(e_i, [s_r, o_i]); w_h)$ 
3. Calculate attention score and its softmax value:
    $a_i = f_a(e_i; w_a)$ 
4. Calculate weighted feature of each obstacle:
    $[softmax(a_i)] \cdot h_i, i \in 1, 2, \dots, N$ 
5. Pool weighted feature of obstacles by LSTM:
    $S_o^{aw} = LSTM[softmax(a_i) \cdot h_i], i \in 1, 2, \dots, N$ 
6. Obtain input data  $S^{aw}$  for prediction net:  $S^{aw} = [s_r, S_o^{aw}]$ 
//Prepare policy distribution and its logit value
7. Calculate policy distribution and its logit value:
    $\text{log} p, p \leftarrow f_p(S^{aw})$ 

```

---

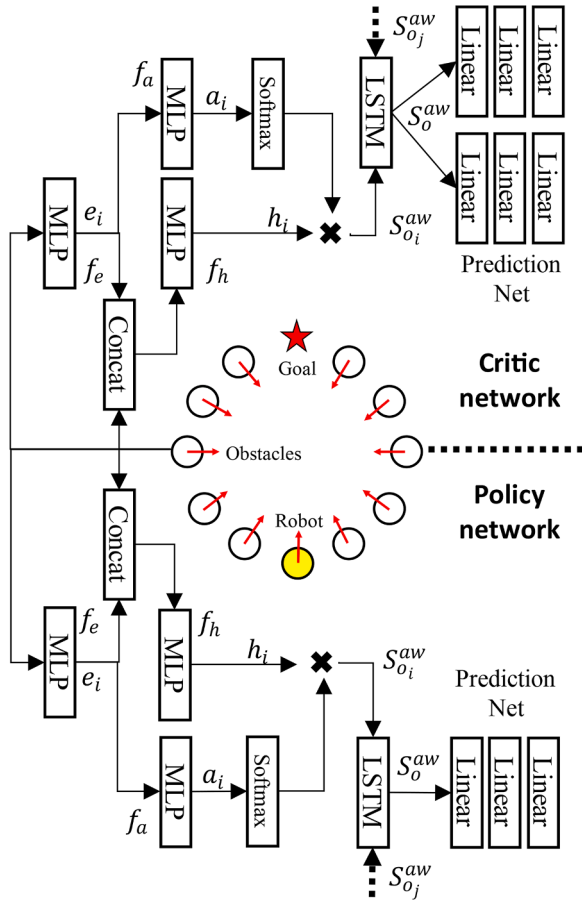


**Fig. 5.** Network framework of our LSA-DSAC. The framework of LSA-DSAC consists of the critic network and policy network. The critic network or policy network receives the same environment features from the circle-crossing simulator for the training. Both critic network and policy network consist of feature interpretation part and prediction part. The feature interpretation part is our LSA encoder which translates features of the robot and obstacles into the attention-based environment features  $S^{aw}$ . Attention-based environment features  $S^{aw}$  is the combination of the robot feature  $s_r$  and attention-based obstacle features  $S_o^{aw}$ . Attention-based environment features  $S^{aw}$  are then fed into prediction networks which are the linear neural layers. Double prediction networks are used in the critic network to reduce the overestimation of Q value, while single prediction network is used in the policy network.

planning strategies. These six strategies include *full-bypass*, *partly-bypass*, *follow-pass*, *wait-pass*, *back-pass*, and *cross*. Their features and examples are shown in Table 4 and Fig. 8. For each algorithm, we sampled 50 trajectories from 500 tests and found that the most of sampled

trajectories of the SARL and Our LSA-DSAC followed the high-quality full-bypass and partly-bypass strategies (Table 5), while the trajectories of the CADRL, LSTMRL, LSTM-A2C, and RG-DSAC followed the medium-quality follow-pass, wait-pass, and back-pass strategies. CADRL and ORCA took low-quality cross strategy that caused more collisions, although the cross strategy led to fast speed sometimes. Fig. 9 presents some examples that indicate the superiority of our LSA-DSAC in trajectory quality when comparing with the state-of-the-art.

**Quantitative evaluation.** The quantity here refers to the statistical motion planning result in 500 tests of each algorithm from the perspectives of the *success rate*, *time to goal*, *collision rate*, *timeout rate* (allowed time 25 s), *mean distance of robot and obstacle*, and *mean reward*. The success rate means the rate to reach the goal. The time to goal means the time to reach the goal if the robot succeeds reaching the goal. The collision rate means the rate to collide with obstacles. The timeout rate means the rate of not reaching the goal given the allowed time limit (25 s). The mean distance of robot and obstacle means the average distance of robot and obstacles if the distance of robot and obstacles is under an alerting slot (e.g., 0.2 m). The mean reward means the average reward received in one episode. This indicator is decided by the reward function. The statistics (Table 6) shows that our LSA-DSAC outperforms the state-of-the-art in all perspectives, except for the time to goal. However, LSA-DSAC still maintains high performance (2nd place) in the time to goal. Despite of this, our LSA-DSAC still performs best among the trainable state-of-the-arts. ORCA slightly outperforms LSA-DSAC regarding the time to goal, but it takes an aggressive strategy that results in a low success rate, more collisions to obstacles and a closer distance to the obstacles.

**Time complexity evaluation.** Here the time complexity is scaled by the *time cost* of each algorithm in training. Online learning algorithm LSTM-A2C learns from online data. Hence, it takes less time 0.42 h in training (Table 7), while other off-policy algorithms including our RG-DSAC and LSA-DSAC take much time. However, our LSA-DSAC and RG-DSAC still keep high performance (around 4 h) when comparing with other off-policy algorithms.

**Transferability evaluation.** The transferability here refers to the performance of a trained model (trained in circle-crossing simulator) in a *new* environment (square-crossing simulator, Fig. 10). The square-crossing environment means the obstacles are randomly generated on the left/right side of environment and move towards random goals on the opposite side. The test results (Table 8) show that our LSA-DSAC keeps the best performance among all trained models in the success rate, mean distance of the robot and obstacle, and mean reward. For the time to goal, collision rate, and timeout rate, our LSA-DSAC has less difference to the best results. Given the results, we can notice that our LSA-DSAC is more likely to take a safe motion planning strategy, as it maintains a safer and preferred distance to the obstacles (0.14 m) where we set the preferred distance to obstacles to be 0.15 m. This results in an efficient and safe motion planning. The time to goal (10.95 s) is almost the same as that of training (10.94 s). This means LSA-DSAC keeps its performance in training if the new simulator (square-crossing) generates similar environment as that of old simulator (circle-crossing). New simulator, at the same time, means generating different/unseen environment (e.g., hostile obstacles). This may result in the degradation of motion planning performance. Despite of this, LSA-DSAC still maintains a high success rate (0.93) that outperforms all state-of-the-arts.

**Robustness evaluation.** The robustness here denotes the *stability* of a trained model in a new environment. The stability is described as the *value changes* (the changes of the statistical results in the quantitative evaluation). Table 9 presents the value changes of these models from the circle-crossing simulator to the square-crossing simulator. Although our LSA-DSAC does not perform best among all trained models, it still keeps high performance (2nd, 2nd, 3rd, 3rd, 2nd, and 4th place respectively).

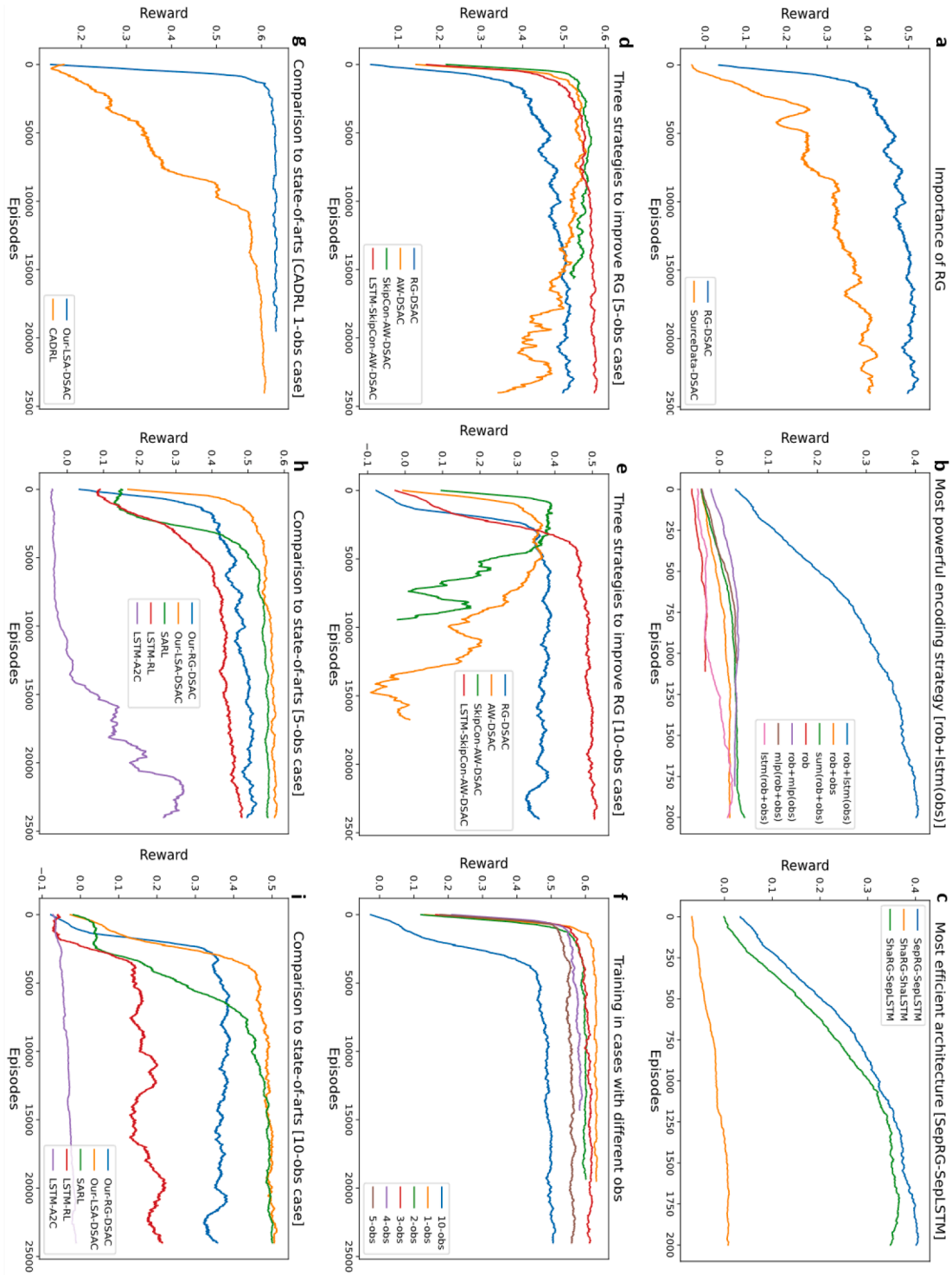


**Fig. 6.** The training curves of our algorithms and state-of-the-art. (a) denotes that the environment state interpreted by the relational graph contributes more to the convergence of DSAC than the source environment state. (b) denotes that after acquiring the robot and obstacle features interpreted by the relational graph, the obstacle features should be encoded by the LSTM. Then, the robot features concatenate the LSTM-encoded obstacle features to form new features for the learning of DSAC. This method of preparing new features outperforms the rest of the methods in improving the convergence of DSAC. (c) denotes that the network architecture with the separate relational graph and separate LSTM (Fig. 5) contributes more to the convergence of DSAC than the architecture with the shared relational graph or share LSTM. (d-e) denotes that the feature interpretation based on the relational graph partly represents the relationship between the robot and the obstacles, resulting in a slow convergence of DSAC. The attention weight or attention network focuses on and precisely describes the relationship between the robot and the obstacles, resulting in a fast convergence of DSAC. However, attention weight is unstable in the training, and the unstable training problem can be mitigated by applying the skip connection method and LSTM method. (f) denotes that the convergence of LSA-DSAC becomes slow, with the increase of the dynamic obstacles in the environment. (g) denotes the comparison of LSA-DSAC and CADRL in convergence. CADRL does not support multi-agent training, therefore the comparison of LSA-DSAC and CADRL is presented in a separate figure. (h-i) denotes the comparisons of LSA-DSAC, RG-DSAC, and the state-of-the-arts that support multi-agent training.

**Table 1**  
Parameters and hyper-parameters of LSA-DSAC.

Parameters/Hyper-parameters	Values of Parameters/Hyper-parameters
LSTM hidden size	50
Number of MLP layer	3
ReLU layer after MLP	Yes (First MLP layer)
MLP input/output size (interaction and embedded layers)	[150, 100]-[100, 50]
MLP input/output size (attention layer)	[100, 100]-[100, 1]
Reward	Source reward
Gamma	0.95
Tau	0.005
Learning rate	3e-4
Alpha	0.2
Frequency of network update	Per step
Automatic entropy tuning	True
Batch size	128
Input layer size (DSAC network)	6 + 50
Hidden layer size (DSAC network)	128
Output size of policy network (DSAC network)	81

**Table 2**  
Converged reward of the models in training with five dynamic obstacles. ORCA is not trainable, therefore it is not included in the comparisons. CADRL does not support multi-agent training, and the converged result of CADRL is from the training with one dynamic obstacle.

Algorithms	Converged reward
ORCA [11]	—
CADRL [33]	0.61(training with one obstacle)
LSTM-RL [18,13]	0.49
SARL [18]	0.55
LSTM-A2C [35,14,34]	0.30
Our RG-DSAC	0.50
Our LSA-DSAC	<b>0.57</b>

#### 4.4. Physical implementation

This paper provides a demonstration of physical implementation. The motivation for physical implementation is to provide a possible way to implement the physical robot and enable the robot to navigate in

dense and dynamic scenarios as the motion planning in the simulator. This paper emphasizes the evaluations of motion planning algorithms in simulators, instead of the evaluations in the real world, because simulators can provide as many tests as possible to extensively evaluate the performance of motion planning algorithms. Moreover, the errors introduced by simulators are predictable.

**Challenges:** When transferring RL algorithm to the real world, the fundamental challenges are the *unexpected observation/measurement errors* and *human operation errors* that may result in an unfair environment when evaluating the motion planning performance of algorithms. For example, the false operations from humans and the observation errors from the sensors may make the results of the real-world evaluations different from that in simulators under the same settings.

**Potential solutions:** This paper attempts to create a real-world environment that has the same settings as that of simulators to demonstrate the motion planning performance of algorithms. The unexpected errors from the real world are not considered in the physical implementation. The problems of unexpected errors are expected to be quantified and mitigated by integrating the model-based methods or Bayesian inference into the model-free RL. For example, in Bayesian context, the environment state is assumed to be the hidden state consisting of observation and noise. The observation errors and human operation errors can be modeled as noise model. The environment state is also captured by certain model like Gaussian. The environment state is described as the mean value and variance. Bayesian method like Bayesian optimization will optimize the model of environment state

**Table 3**  
Interpretability (explainable ability) evaluation. Here the interpretability is measured by whether there are post-training indicators generated to justify the actions or policies.

Algorithm	Interpretability (explainable ability)
ORCA	—
CADRL	No
LSTMRL	No
SARL	Yes
LSTM-A2C	No
RG-DSAC	No
LSA-DSAC	<b>Yes</b>

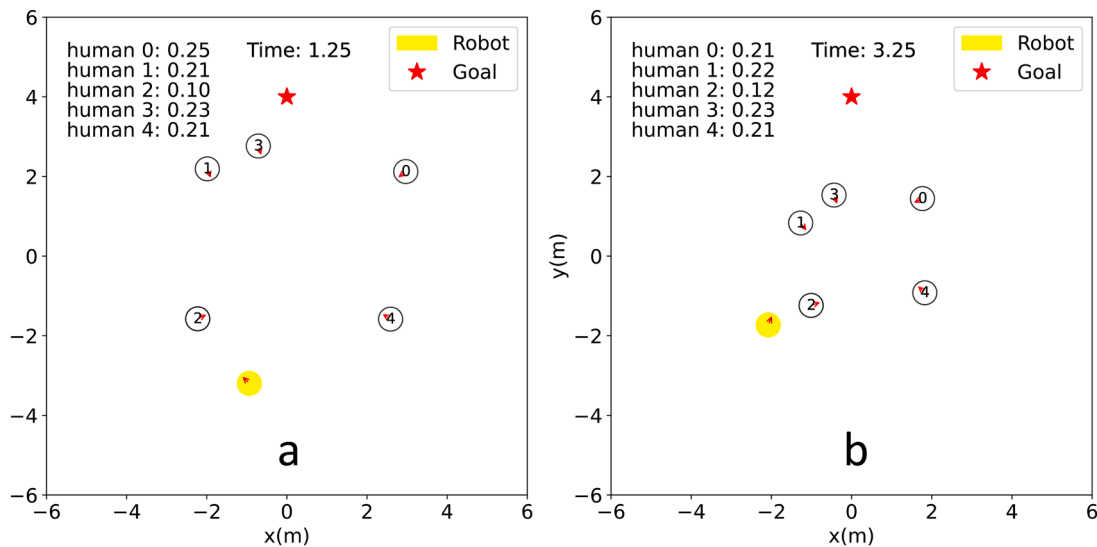


**Fig. 7.** Examples of obstacles with attention score in LSA-DSAC. The human here denotes the dynamic obstacles. The distance between the robot and obstacles is not so important to decide the attention score sometimes, such as the human (obstacle) 2 in (a) and (b). The obstacles heading toward the robot, such as human 0, are expected to have a higher attention score, but it doesn't mean only the direction of the obstacle decides the attention score. Attention score is an overall evaluation that considers the direction of motion, speed, and distance between the robot and the obstacles. Hence, in (b), human 0 has a high attention score, but its attention score is slightly smaller than that of human 1 and human 3.

**Table 4**  
Features of six motion planning strategies. The motion planning strategy here is defined by humans according to human experience.

Strategy	Description	Speed	Collision
Full-bypass	Bypass all obstacles	Fast	Less
Partly-bypass	Bypass most obstacles	Fast	Less
Follow-pass	Follow front obstacles and pass	Medium	Less
Wait-pass	Wait until obstacles move away and pass	Slow	Less
Back-pass	Move back until obstacles move away and pass	Slow	Less
Cross	Cross dense obstacles	High/Medium/Slow	More

towards minimizing the variance. Therefore, unexpected observation errors and human operation errors are quantified, and the environment state is more accurate. However, the model-based methods may bring new problems like expensive computation and inaccurate surrogate model [45]. This paper is not going to extend this topic, but model-based methods may be considered in future works for motion planning in dense and dynamic scenarios.

In the physical implementation, the models of trainable motion planning algorithms are trained with the data from the simulator, while the testing data is collected by the robot sensors from the real world. The mechanism of physical implementation is as follows: A Local area network (LAN) is established in the robot operation system (ROS) [46]. Agents in the experimental area are connected to the LAN. They are

equipped with a marker point that can be captured by cameras to create a rigid body model in the motion capture system. The workflow in the physical implementation is shown in Fig. 11a. First, cameras capture the agent's location information (observations) via marked points. Second, observations are sent to the host to compute the agent's actions by the RL model and ORCA. Third, the actions are broadcasted to the agents by WiFi. Finally, the actions are executed by agents. Once the robot reaches the goal, the task is finished.

In action execution (Fig. 11b), Jetson Nano converts digital actions to ROS messages. Stm32 then computes the wheel speed using ROS messages and converts it into messages of Pulse-Width Modulation (PWM). They can be recognized and executed by motors. The motion capture system is based on optical tracking technology [47–49] to localize agents. It consists of eight 3D cameras. Finally, our physical implementation is tested in both a ROS Gazebo environment and the real

**Table 5**  
Qualitative evaluation. The quality here is measured according to the efficiency or the property of learned motion planning strategies.

Algorithm	Learnt motion planning strategy
ORCA	Cross
CADRL	Cross/Follow-pass
LSTMRL	Partly-bypass/Follow-pass
SARL	Full-bypass/Partly-bypass
LSTM-A2C	Back-pass/Wait-pass
RG-DSAC	Partly-bypass/Follow-pass
LSA-DSAC	<b>Full-bypass/Partly-bypass</b>

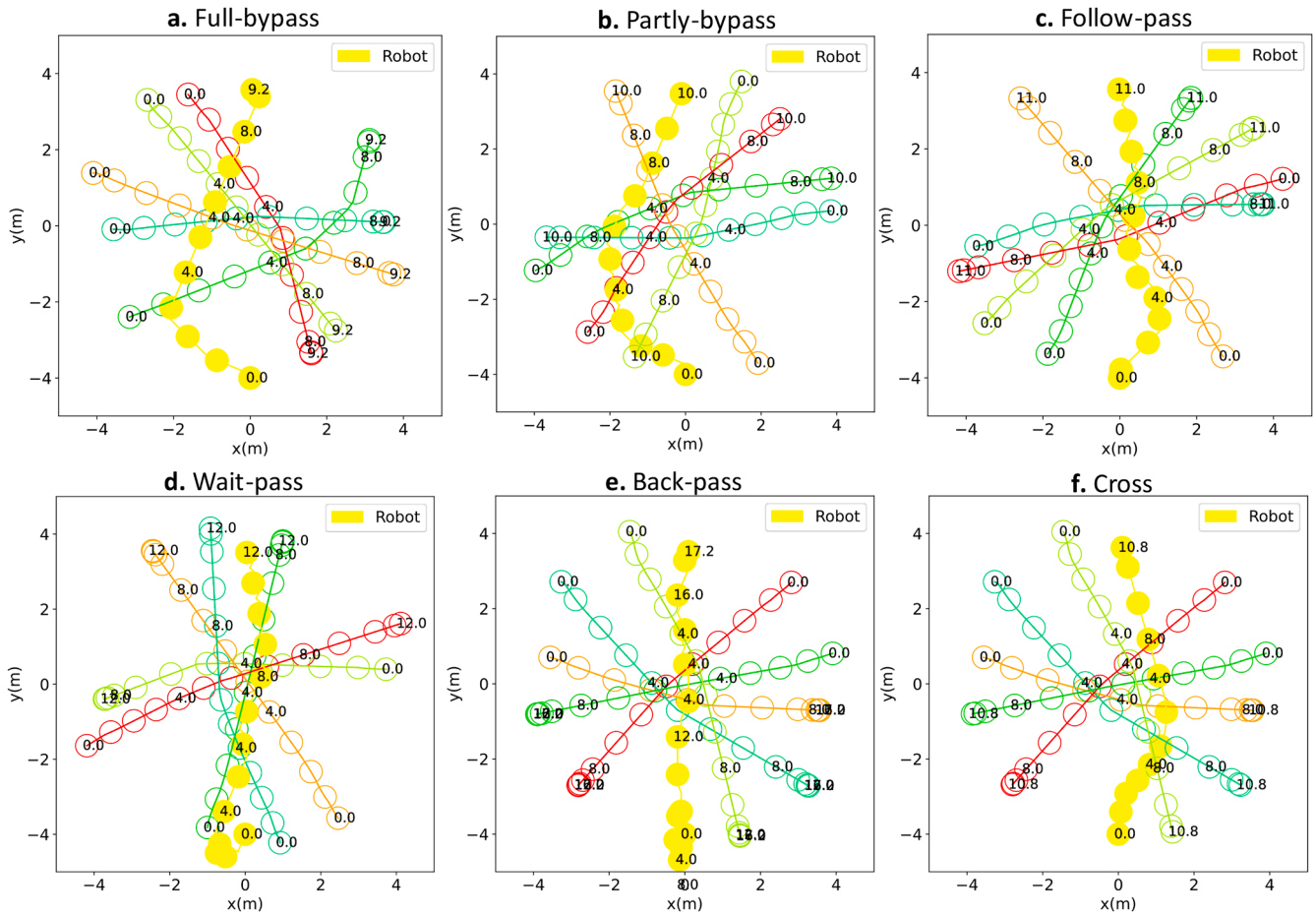


**Fig. 8.** Six learned motion planning strategies. The numbers along the trajectories represent the time step of each robot or obstacle. The full-bypass and partly-bypass are the most efficient motion planning strategies. The performance of wait-pass and follow-pass strategies is acceptable. The back-pass is the most time-consuming motion planning strategy. The cross strategy is efficient in the motion planning sometimes, but it causes many collisions.

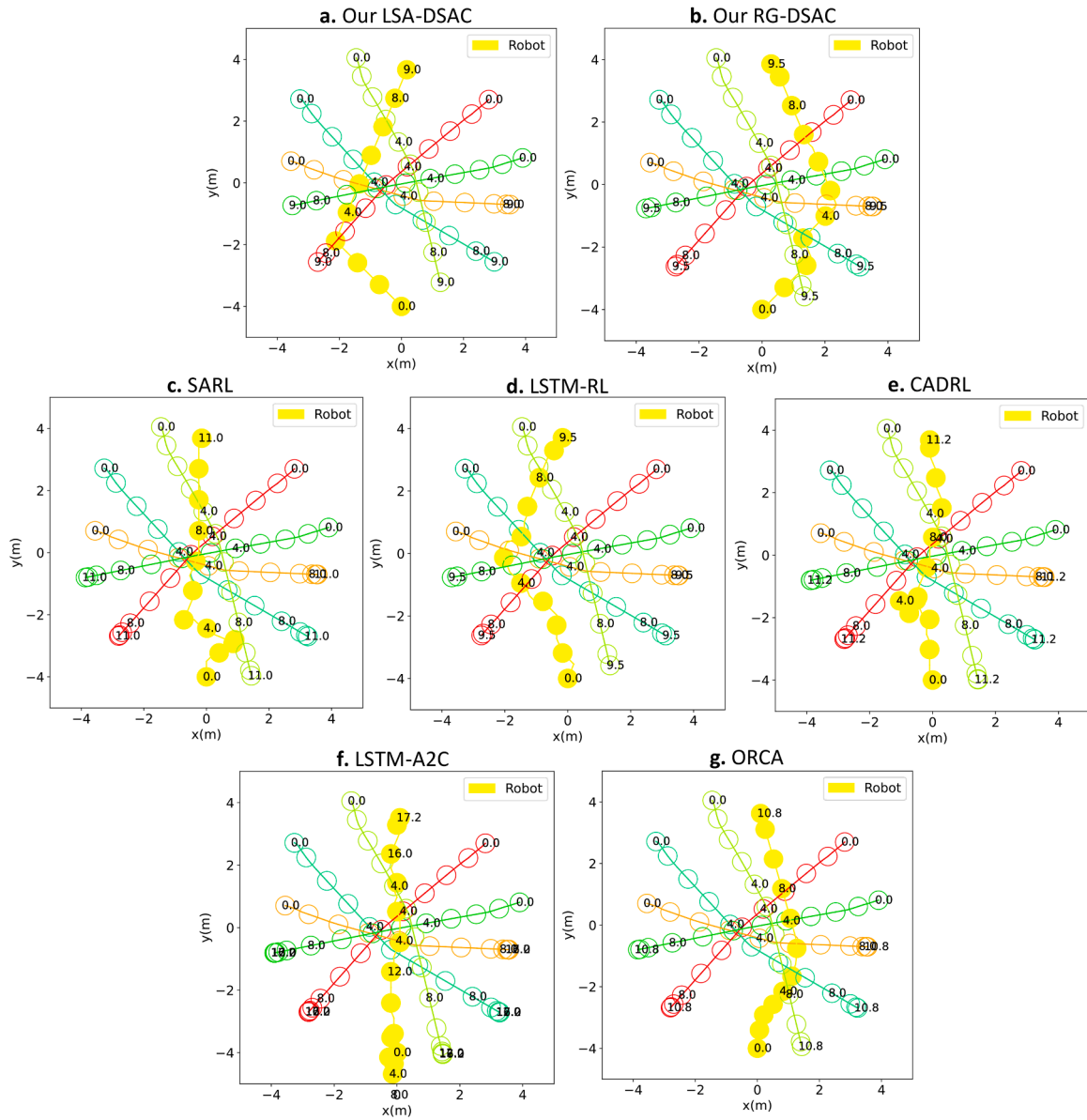


Fig. 9. Superiority of LSA-DSAC in trajectory quality. Here this paper presents an example that demonstrates a good performance of our LSA-DSAC in the time cost to reach the goal.

Table 6  
Statistical results of the quantitative evaluation.

Algorithms	Success rate	Time to goal	Collision rate	Timeout rate	Mean distance (m)	Mean reward
ORCA	0.43	10.86	0.564	0.006	0.08	—
CADRL	0.89	11.30	0.106	0.004	0.16	0.47
LSTMRL	0.96	12.10	0.02	0.01	0.16	0.49
SARL	0.99	10.96	0.01	0.00	0.18	0.56
LSTM-A2C	0.88	17.04	0.05	0.07	0.12	0.36
RG-DSAC	0.94	11.37	0.06	0.00	0.14	0.52
LSA-DSAC	<b>0.996</b>	<b>10.94</b>	<b>0.004</b>	<b>0.00</b>	<b>0.15</b>	<b>0.57</b>

world (Fig. 11c). Videos of the ROS Gazebo test and the real-world tests are available as follows:

- 1) Gazebo test (Fig. 12). The video link is available at <https://youtu.be/A-GdHGoWwCk>. The purpose of the Gazebo test is to compare the motion planning differences between the Gazebo environment

Table 7  
Time complexity evaluation. The time complexity here is measured by the time cost of all algorithms in training in 5-obstacle case.

Algorithms	Time cost (hour/10 K epi.)
ORCA	—
CADRL	7.4 (train with one obstacle)
LSTMRL	16.08
SARL	14.72
LSTM-A2C	0.42
RG-DSAC	4.38
LSA-DSAC	4.56

and the simulator. The same trained models are evaluated in Gazebo environment and the circle-crossing simulator. The experiment demonstrates that the motion planning performance in Gazebo environment and circle-crossing simulator is almost the same under the same settings. Their difference is that the trajectories of the robot and the obstacles in Gazebo environment are not as smooth as that of the circle-crossing simulator, given the video demonstration. The

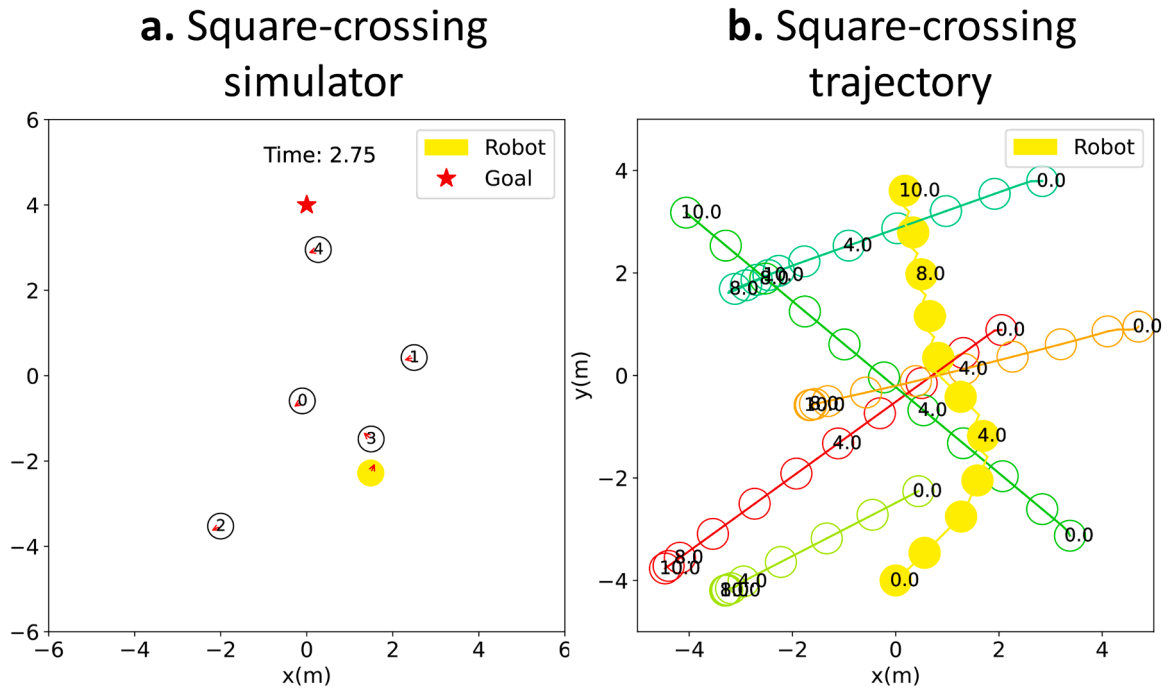


Fig. 10. An example of 500 tests in the square-crossing simulator. (a) presents the simulator, while (b) presents the trajectories of the robot and obstacles at the end of an episode. The square-crossing simulator is only used in transferability evaluations.

Table 8

Transferability evaluation. Here the transferability is measured by the performance of trained models (training in the circle-crossing simulator) in the new environment (the square-crossing simulator). The performance here is measured using the same metrics as that of quantity evaluation.

Algorithms	Success rate	Time to goal	Collision rate	Timeout rate	Mean distance (m)	Mean reward
ORCA	0.74	9.12	0.256	0.004	0.08	—
CADRL	0.88	11.19	0.01	0.11	0.17	0.48
LSTMRL	0.91	10.54	0.03	0.06	0.12	0.49
SARL	0.92	10.96	0.02	0.06	0.17	0.51
LSTM-A2C	0.45	15.61	0.41	0.14	0.10	0.12
RG-DSAC	0.40	11.09	0.59	0.01	0.11	0.10
LSA-DSAC	<b>0.93</b>	10.95	0.05	0.02	<b>0.14</b>	<b>0.51</b>

sensor errors of Gazebo environment cause the positioning drift, reducing the smoothness of the trajectories. However, the robot can still reach the destination safely and efficiently by learning an efficient motion planning policy and keeping a safe distance to the obstacle.

- 2) Real-world test in the static environment (Fig. 13). The video link is available at the website <https://www.youtube.com/watch?v=bH5FbA14AqE>. The model tested in Gazebo environment is then tested in the static real-world environment. Given the test result, the

Table 9

Robustness evaluation. Here the robustness is measured by the value changes of trained models from the circle-crossing simulator to the square-crossing simulator. Robustness evaluation uses the same metrics as that of quantity evaluation.

Algorithms	Success rate	Time to goal	Collision rate	Timeout rate	Mean distance (m)	Mean rewards
ORCA	0.310	1.560	0.308	0.002	0.000	—
CADRL	0.010	2.110	0.096	0.106	0.010	0.02
LSTMRL	0.078	1.160	0.008	0.050	0.020	0.04
SARL	0.070	0.000	0.010	0.060	0.010	0.05
LSTM-A2C	0.430	1.430	0.360	0.070	0.020	0.24
RG-DSAC	0.540	0.280	0.530	0.010	0.030	0.42
LSA-DSAC	0.066	0.010	0.046	0.020	0.010	0.06

robot can reach the destination and avoid all obstacles simultaneously.

- 3) Real-world test in dense and dynamic scenarios (Fig. 14). The video is available at <https://youtu.be/UB6aC3XoZ6c>. The real-world test in dense and dynamic scenarios uses the same model as the above two tests. Given the test result, the robots can reach their destinations and avoid all dynamic obstacles simultaneously. As Gazebo test, real-world tests in static and dynamic scenarios have the same problem in the positioning drift caused by the sensor errors, reducing the smoothness of the trajectories, given the video demonstration. However, the robot can still reach the destination safely and efficiently by learning an efficient motion planning policy and keeping a safe distance from the obstacle.

## 5. Discussions

### 5.1. Unstable training of aw-dsac

The unstable training of AW-DSAC is discussed in this section. We reconstruct the trainings of AW-DSAC and our LSA-DSAC with different seed and trace the relevant mediate values in cases with 5 and 10 obstacles respectively, as Fig. 15.

Given the reward values in Fig. 15, we can see that AW-DSAC diverges with the training in 5-obstacle case and stops in the training in 10-obstacle case due to zero gradient received, while our LSA-DSAC is

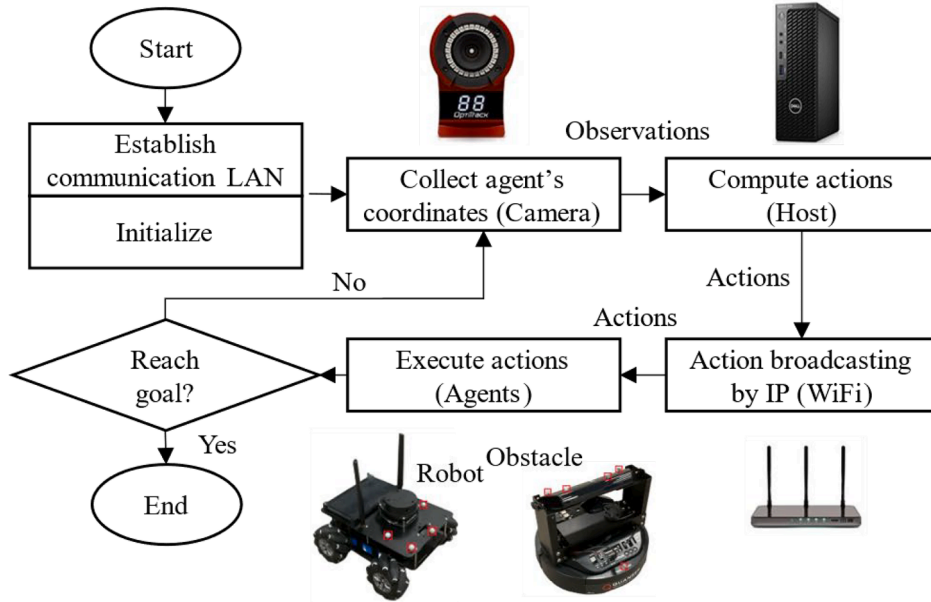
unlikely to suffer from this problem that can be easily classified to be typical “vanishing gradient” problem. Given the loss values of critic networks, AW-DSAC and LSA-DSAC converges well, and less difference exists.

Given the loss values of policy networks, our LSA-DSAC receives and converges to a reasonable loss value. However, AW-DSAC faces two cases in the loss values: *high-zero loss*, and *zero loss*. The high-zero loss means AW-DSAC receives a higher or reasonable loss value that results in good convergence at the beginning, but later the loss value drops to

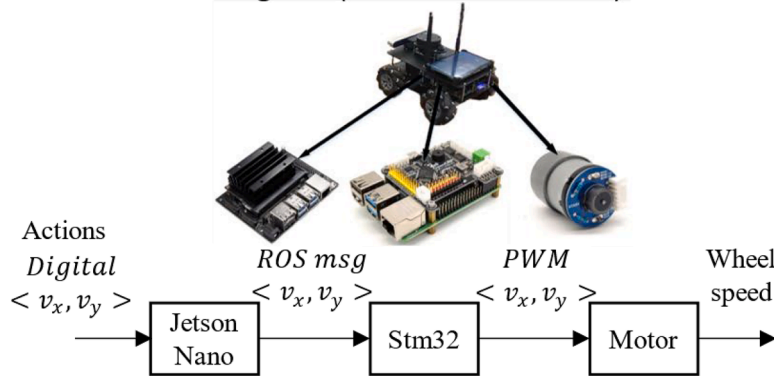
zero that results in vanishing gradient. The zero loss means AW-DSAC receives zero policy loss at the beginning of training, resulting in vanishing gradient directly.

Given the values of alpha loss and alpha, we can see that alpha losses of AW-DSAC and LSA-DSAC haven’t converged. This results in the drop the alpha value. Consequently, the entropy term of DSAC contributes less to the loss value with the training, and DSAC relies on the reward gradually to compute the loss value, like the classical off-policy actor critic. The reason for this result is in the setting of target entropy. Let

**a. Workflow of physical implementation**



**b. Action execution in agents (robot and obstacles)**



**C. Motion capture system, gazebo and real-world tests**

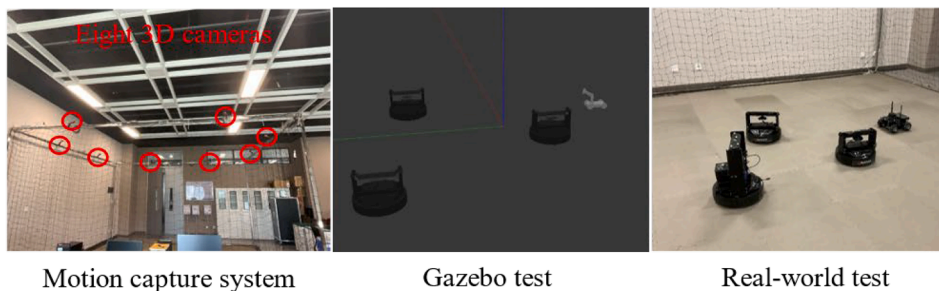


**Fig. 11.** Details of physical implementation. (a) presents the detailed steps of physical implementation. (b) presents the hardware of the robot and obstacles for the action execution. (c) presents the motion capture system and an example of the tests in the gazebo and the real world. The motion capture system localizes the robot and obstacles in real-time to compute the positions and velocities of the robot and obstacles.

recall the equation of loss value of alpha  $\mathcal{L}_\alpha = -\min[\log\alpha(\overline{\mathcal{H}} - \mathcal{H})]$ , the divergence of alpha loss means the entropy  $\mathcal{H}$  cannot reach fixed target entropy  $\overline{\mathcal{H}} = \log|\mathcal{A}|$  where  $\mathcal{A}$  is the action space. The consequence is a faster drop of alpha value and DSAC relies on reward for gradient update too early. This little flaw exists when SAC is adapted into discrete action space, and it remains unsolved. Some early stage works attempt to make the target entropy adaptive [50], but the solutions cannot be generalized but lack theoretical proofs.

Despite of a dropping alpha value, it doesn't mean DSAC cannot converge well. We can see that our LSA-DSAC still has a good convergence, but AW-DSAC suffers from the problems of high-zero loss and zero loss as we discussed above. Given Fig. 15, alpha value drops to near zero after 100–200 episodes, but AW-DSAC suffers from vanishing gradient after 2k episodes. This indicates that a faster dropping alpha is not the reason for the divergence of AW-DSAC (note that alpha is also dropping in normal case where alpha loss converges). The attention mechanism or the combination of attention and DSAC more likely relates to divergence or vanishing gradient. Let recall the policy loss  $\mathcal{L}_{oss_p} = -\text{mean}[\mathbb{E}_{s \sim p}[Q(s)] + \alpha \cdot \mathcal{H}(\pi(\cdot|s))]$  where  $\mathbb{E}_{s \sim p}[Q(s)] = \sum \min[(Q(s)_{c1}, Q(s)_{c2}) \cdot p]$ . The policy loss is related to  $\sum \min[(Q(s)_{c1}, Q(s)_{c2}) \cdot p]$  because  $\alpha \cdot \mathcal{H}(\pi(\cdot|s))$  moves close to zero. In  $\sum \min[(Q(s)_{c1}, Q(s)_{c2}) \cdot p]$ , the critic value and policy value are computed by  $f(S^{aw})$  where  $f(\cdot)$  is the critic network or policy network and  $S^{aw}$  is the embedding via attention network. We assume that 1) a deep network  $f(\cdot)$  where the attention network is included, results in lost feature of  $S^{aw}$  and consequent slow convergence, and 2) the sum operation is not injective, and results in further lost feature of  $S^{aw}$  as we presented in Section 3.4. To support our two assumptions, we integrate skip connections to attention network. Consequently, the convergence improves, and this supports our assumption, but AW-DSAC still has the problem of vanishing gradient. Then, we replace the sum operation with LSTM that keeps more feature, and most important, LSTM can stabilize the training due to its activation function (identity function) that makes the gradient of LSTM constant. Therefore, the final policy loss of LSA-DSAC can converge. However, LSTM requires time to converge at the beginning of training. This is the reason why LSA-DSAC converges slightly slower than that of AW-DSAC

in 5-obstacle case. AW-DSAC suffers from vanishing gradient early or late where this problem becomes apparent with the increase of obstacle numbers.

## 5.2. The computation challenges for LSA-DSAC under the context of increasing obstacle numbers

**Challenge of time cost in training.** For a fair comparison, we recorded the time cost of our LSA-DSAC in the first 10 K episodes in the cases of 1, 2, 3, 4, 5 and 10 obstacles (Table 10), because LSA-DSAC almost converges in the first 10 K episodes. We can notice that the time cost of training is increasing with the increase of obstacle numbers. We think two reasons for the increasing time cost: 1) increasing numbers of input features, and 2) increasing task complexity.

An increasing numbers of input features means the increase dimensions of input matrix. The multiplication of input matrix and weight matrix of deep network (including MLPs and LSTM, especially LSTM) takes more time to compute the results. This slows down the training and inference speed. However, in our work, we defined necessary features of the robot and obstacles, instead of using image-based input, therefore the dimension of input matrix is acceptable, and it has limited impacts to the training and inference speed (see the time cost in cases of 1, 2, and 3 obstacles where the training takes almost the same time). With the increase of task complexity (obstacle numbers), the robot is likely to take more steps for exploration in each episode to find the goal. More steps mean more frequent use of deep networks that dramatically increase the time cost (see the time cost in cases of 3, 4, 5, and 10 obstacles).

We also compared the time cost of LSA-DSAC with other carefully selected algorithms when the obstacle number increases. These algorithms include RG-DSAC (relational graph combines with DSAC), SARL (attention network combines with DQN), and LSTMRL (LSTM combines with DQN) (Table 11). We think the challenge of time cost should be evaluated from two perspective: *average time cost* and *growth rate of time cost with increasing obstacle number*. After comparisons, we concluded that all algorithms for comparisons face the computation challenge from increasing obstacle number, but with different average time cost and

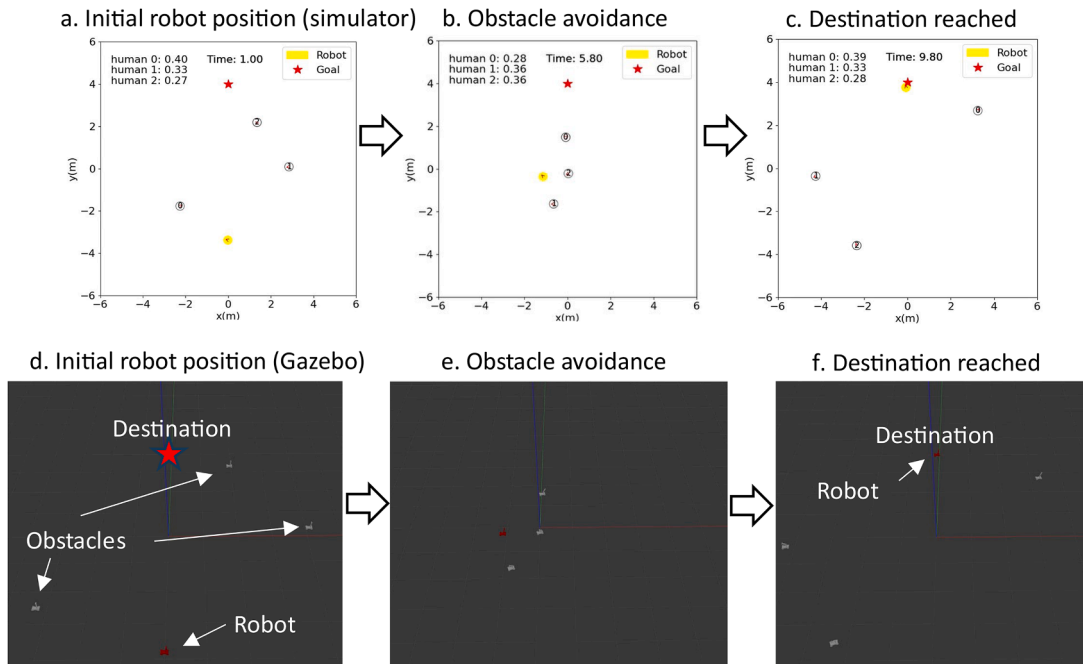


**Fig. 12.** The Gazebo test. The same trained models are evaluated in Gazebo environment and the circle-crossing simulator simultaneously. The robot and obstacles in these two environments are controlled by the LSA-DSAC and ORCA respectively. The model of LSA-DSAC is trained by 1k episodes in the circle-crossing simulator. Finally, the motion planning results in these two environments were almost the same, despite a few differences in the smoothness of the trajectory given the video results.

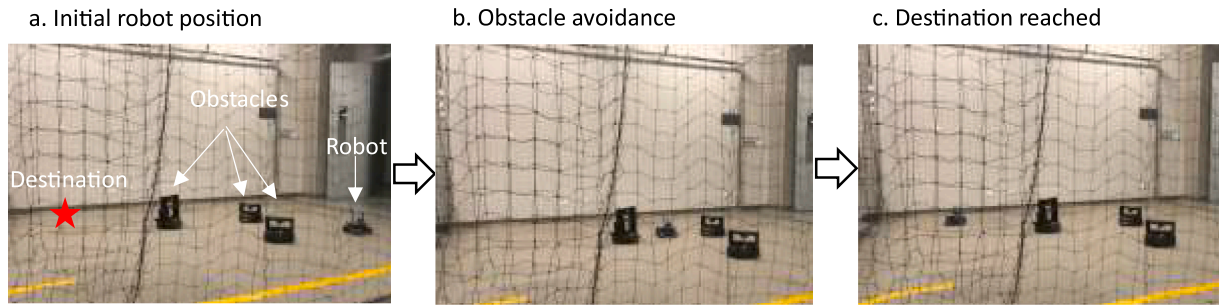


**Fig. 13.** The real-world test in the static environment. As Gazebo test, the real-world test in a static environment uses the model of LSA-DSAC. The model of LSA-DSAC is trained by 1k episodes in the circle-crossing simulator. The obstacles spread along the robot’s route to the destination. Finally, the robot reached its destination and avoided all obstacles simultaneously.

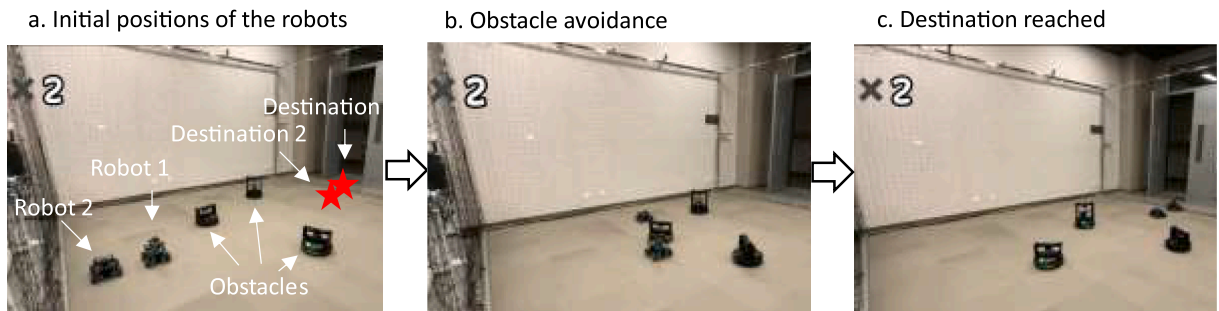


**Fig. 14.** Real-world test in dense and dynamic scenarios. As Gazebo test and real-world test in a static environment, real-world test in dense and dynamic scenarios uses the model of LSA-DSAC. The model of LSA-DSAC is trained by 1k episodes in the circle-crossing simulator. Two robots use the same model of LSA-DSAC. Each robot treats another robot as an obstacle in the motion planning task. The obstacles spread along the robot’s routes to their destinations and randomly walk continuously. Finally, the robots reached their destinations and avoided all dynamic obstacles simultaneously. Note that this paper omitted the real-world test in dense and dynamic scenarios with one robot because each robot treats another robot as an obstacle in the motion planning.

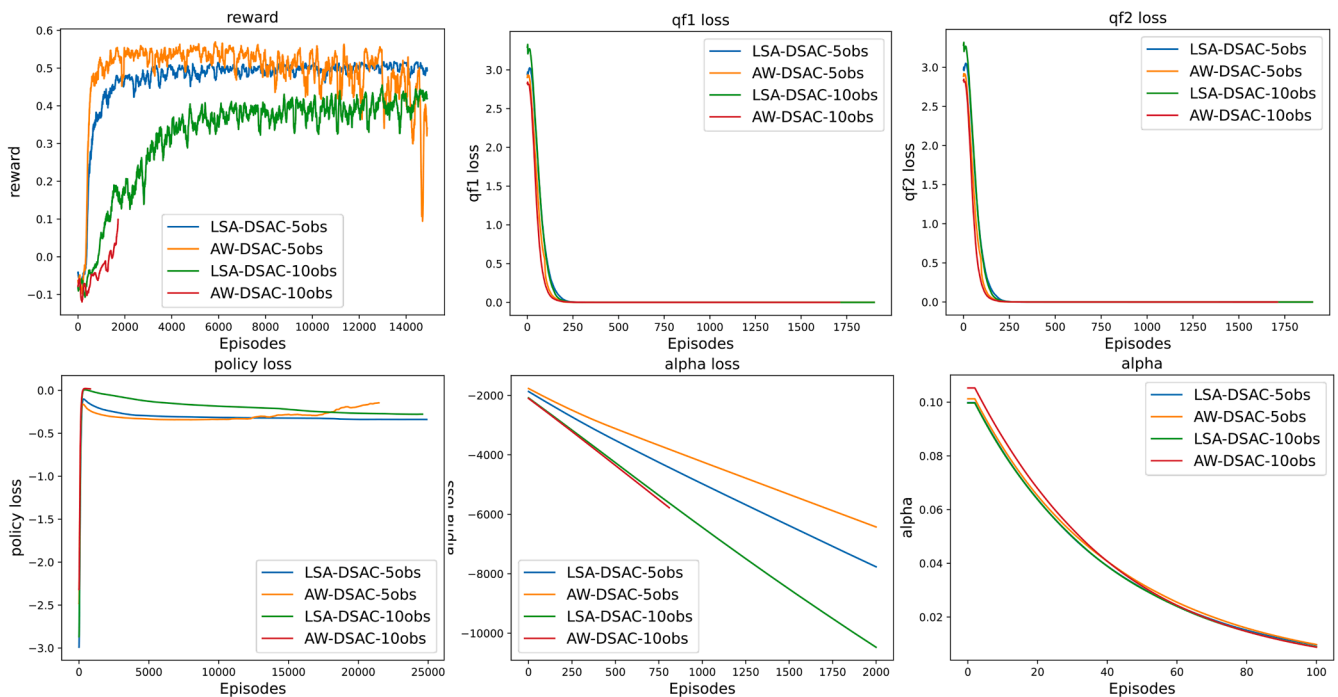


**Fig. 15.** The training experiments of AW-DSAC and LSA-DSAC with different seed and mediate values that include the loss value of critic network, loss value of policy network, loss value of Alpha, and Alpha value.

growth rate. Specifically,

- 1) LSTM suffers more from increasing obstacle number than attention network, given the growth rate comparisons of SARL and LSTMRL.
- 2) Relational graph is likely to bring more average time cost and higher growth rate of time cost, given the comparisons of LSA-DSAC and RG-DSAC.
- 3) For LSA-DSAC, DSAC can significantly reduce the average time cost, but LSTM in LSA will result in higher growth rate, given the comparisons of LSA-DSAC, SARL, and LSTMRL.

**Challenge of memory consumption due to LSTM.** Given the mechanism of LSTM, it is obvious that for complex tasks involving long time series (more time steps in each episode) or large numbers of input features (obstacle numbers), the memory demands can become significantly elevated in our LSA-DSAC. This extreme case should be avoided.

In our experiment, we constrained the maximum time cost for one task is 25 s (100 steps) to trade-off the exploration and computation (due to long time series/time steps), therefore guaranteeing sufficient exploration for RL training and acceptable computation. The experiments from 0 to 500 episodes indicate that the memory cost *slightly* increases with the increase of obstacle numbers. Therefore, the challenges from memory cost can be ignored when the obstacle number and step number of exploration are small. However, in the case with *hundred/thousand obstacles and no constraints on exploration steps*, the memory cost would be huge and cannot be ignored. We think there are two promising solutions for addressing this challenge:

- 1) The combination of global path planning and local motion planning. The ego observations are collected where limited number of obstacles near the robot are considered to prepare the observation. Global path planning algorithm is responsible for finding local goals for local motion planning. Therefore, the challenge of long time series and large numbers of input features are better avoided.
- 2) Designing hierarchical RL where complex tasks are decoupled into simple subtasks. High-level policy of hierarchical RL is responsible for decoupling long-term task into simple subtasks. Low-level policy is used for addressing simple subtasks where the dimensions of input features and length of episodic steps are acceptable.

### 5.3. Inaccurate attention of attention networks

Attention network shows great interpretability and potentials to prepare high-quality representation. However, attention network is problematic in the early-stage training. Specifically, attention network is likely to focus on most salient features and ignore some important but unobvious features. This prepares poor representation and makes entire algorithm diverged. In our LSA-DSAC, we try to mitigate this problem by keeping source features as much as possible via replacing sum operation with LSTM encoding. Therefore, some unobvious but important features are unlikely to be overlapped by some salient features.

Other promising solutions are 1) the model-based approach, and 2) meta learning. The model-based approach is to parameterize the weight or attention score of each feature to be an unknown function. Thus, the problem becomes to find the optimal unknown function data as less as possible. The model-based approach is promising to capture this unknown function. For example, Bayesian method like Bayesian optimization takes less sequential data to find the optimal parameters of unknown function. However, model-based methods better suit the low-dimensional inputs, and the high-dimensional case remains to be challenging.

It is also interesting to meta-learn the optimal attention score/weight in different cases via meta learning (e.g., zero-shot meta learning) where various optimal sets of weight/attention score are maintained. Therefore, attention network can be initialized with good weight/attention score when facing the same tasks, instead of training from the scratch.

**Table 10**

The relationship of obstacle number and time cost.

Obstacle numbers in training	Time cost (hour/10 K <i>epi.</i> )	Memory cost (M) from 0 <i>epi.</i> to 500 <i>epi.</i>
1	2.7	321 (1444 to 1765)
2	2.9	300 (1443 to 1743)
3	3.0	315 (1446 to 1761)
4	3.7	325 (1445 to 1770)
5	4.3	333 (1448 to 1781)
10	8.3	355 (1448 to 1803)

## 6. Conclusion

This paper combines representation learning with reinforcement learning for robotic motion planning in the environment with dynamic and dense obstacles. First, relational graph combines with DSAC to form the RG-DSAC, and satisfactory performance of motion planning is achieved. Second, the expressive power of interpreted features is improved by the attention weight (attention network) to replace the relational graph in the feature interpretation. This improves network convergence. Third, the attention weight (network) is optimized by the skip connection method and LSTM to eliminate unstable training. Therefore, the convergence speed and converged result are further improved. Extensive experiments (training and evaluations) of our algorithms and state-of-the-art are conducted. The results demonstrated that our LSA-DSAC outperforms the state-of-the-art in trainings and most evaluations. The details of physical implementation of the robot and dynamic obstacles are also given to provide a possible method to transplant the simulation into the real world. Motion planning experiments were conducted in indoor scenarios (ROS Gazebo environment and real world). This further demonstrates the credibility of our motion planning algorithm and physical implementation method in the real world.

As future research, we may focus on meta learning the weight/attention score of the attention network to further improve stability, convergence, and interpretability. We will also try Bayesian model-based method and zero-shot meta learning in future research. This contributes to better interpretability and stability and reduces unexpected errors once the robot works in the real world, therefore reducing the sim2real gap.

## Funding

Open access funding provided by University of Eastern Finland (UEF) including Kuopio University Hospital.

The physical implementation is supported in part by the National Natural Science Foundation of China under Grant 62003218, Guangdong Basic and Applied Basic Research Foundation under Grant 2019A1515110234, and Shenzhen Science and Technology Program under Grant RCBS20200714114921371.

**Table 11**

The time cost comparison of LSA-DSAC with other algorithms when obstacle number increases.

Obstacle numbers/component /Growth rate	Time cost for LSA-DSAC (hour/10 K <i>epi.</i> )	Time cost for RG-DSAC (hour/10 K <i>epi.</i> )	Time cost for SARL (hour/10 K <i>epi.</i> )	Time cost for LSTMRL (hour/10 K <i>epi.</i> )
5	4.3	4.4	14.7	16.1
10	8.3	12.5	21.2	29.8
Components	LSA (Attention with LSTM) & DSAC	RG & DSAC	Attention & DQN	LSTM & DQN
Growth rate of time cost	91	184	44	85

## CRedit authorship contribution statement

**Chengmin Zhou:** Investigation, Conceptualization, Visualization, Methodology, Data curation, Validation, Formal analysis, Writing – original draft, Software, Project administration. **Xin Lu:** Methodology, Resources. **Jiapeng Dai:** Resources. **Xiaoxu Liu:** Resources, Funding acquisition. **Bingding Huang:** Resources, Supervision, Conceptualization. **Pasi Fränti:** Resources, Conceptualization, Writing – review & editing, Supervision, Funding acquisition.

## Declaration of competing interest

All authors certify that they have no affiliations with or involvement in any organization or entity with any financial interest or non-financial interest in the subject matter or materials discussed in this manuscript.

## Acknowledgement

We thank Shenzhen Technology University, Shenzhen China for providing the resources for physical robot implementation.

## Data availability

Data will be made available on request.

## References

- [1] L. Fuentes-Moraleda, P. Díaz-Pérez, A. Orea-Giner, A. Muñoz- Mazón, T. Villacé-Moliner, Interaction between hotel service robots and humans: a hotel-specific service robot acceptance model (sRAM), *Tour. Manag. Perspect* 36 (October 2020) (2020) 100751.
- [2] B. Gerrits, P. Schuur, Parcel delivery for smart cities: a synchronization approach for combined truck-drone-street robot deliveries, in: 2021 Winter Simul. Conf. (WSC), Phoenix, AZ, USA, 2021, pp. 1–12.
- [3] S. Srinivas, S. Ramachandiran, S. Rajendran, Autonomous robot-driven deliveries : a review of recent developments and future directions, *Transp. Res. Part E* 165 (2022) 102834.
- [4] W.S. Barbosa, et al., Industry 4.0: examples of the use of the robotic arm for digital manufacturing processes, *Int. J. Interact. Des. Manuf.* 14 (4) (2020) 1569–1575.
- [5] M. Bartoš, V. Bulej, M. Bohušík, J. Stancek, V. Ivanov, P. Macek, An overview of robot applications in automotive industry, *Transp. Res. Procedia* 55 (2021) 837–844.
- [6] P.E. Hart, N.J. Nilsson, B. Raphael, A formal basis for the heuristic determination of minimum cost paths, *IEEE Trans. Syst. Sci. Cybern.* 4 (2) (1968) 100–107.
- [7] E.W. Dijkstra, A note on two problems in connexion with graphs, *Numer. Math.* 1 (1) (1959) 269–271.
- [8] J. hwan Jeon, et al., Optimal motion planning with the half-car dynamical model for autonomous high-speed driving, in: 2013 American Control Conference, Washington, DC, USA, 2013, pp. 188–193.
- [9] L.E. Kaviraki, P. Svestka, J.C. Latombe, M.H. Overmars, Probabilistic roadmaps for path planning in high-dimensional configuration spaces, *IEEE Trans. Robot. Autom.* 12 (4) (1996) 566–580.
- [10] D. Fox, W. Burgard, S. Thrun, The dynamic window approach to collision avoidance, *IEEE Robot. Autom. Mag.* 4 (1) (1997) 23–33.
- [11] J. Den Van Berg, M. Lin, D. Manocha, Reciprocal velocity obstacles for real-time multi-agent navigation, in: *Proc. - IEEE Int. Conf. Robot. Autom.* 2, 2008, pp. 100–107.
- [12] X. Dai, Y. Mao, T. Huang, N. Qin, D. Huang, Y. Li, Automatic obstacle avoidance of quadrotor UAV via CNN-based learning, *Neurocomputing* 402 (2020) 346–358.
- [13] V. Mnih, et al., Playing Atari with Deep Reinforcement Learning, *arXiv* (2013) 1–9.
- [14] V. Mnih, et al., Asynchronous methods for deep reinforcement learning, in: *Proceedings of Machine Learning Research* 48, 2016, pp. 1928–1937.
- [15] A. Alahi, K. Goel, V. Ramanathan, A. Robicquet, L. Fei-Fei, S. Savarese, Social LSTM: human trajectory prediction in crowded spaces, in: *2016 IEEE Conference on Computer Vision and Pattern Recognition (CVPR)*, 2016, pp. 961–971.
- [16] C. Chen, S. Hu, P. Nikdel, G. Mori, and M. Savva, “Relational graph learning for crowd navigation,” in *arXiv Preprint*, 2019, pp. 1–7.
- [17] W.L. Hamilton, Graph representation learning, *Synth. Lect. Artif. Intell. Mach. Learn.* 14 (3) (2020) 1–159.
- [18] C. Chen, Y. Liu, S. Kreiss, A. Alahi, Crowd-robot interaction: crowd-aware robot navigation with attention-based deep reinforcement learning, in: *Proc. - IEEE Int. Conf. Robot. Autom.* 2019-May, 2019, pp. 6015–6022.
- [19] A. Vemula, K. Muelling, J. Oh, Social attention: modeling attention in Human crowds, in: *Proc. - IEEE Int. Conf. Robot. Autom.*, 2018, pp. 4601–4607.
- [20] T. Dam, G. Chalvatzaki, J. Peters, and J. Pajarinen, “Monte-Carlo robot path planning,” *arXiv Prepr.*, pp. 1–8, 2022.
- [21] H. Van Hasselt, A. Guez, D. Silver, Deep reinforcement learning with double Q-learning, in: 30th AAAI Conf. Artif. Intell. AAAI 2016, 2016, pp. 2094–2100.
- [22] Z. Wang, T. Schaul, M. Hessel, H. Van Hasselt, M. Lanctot, N. De Freitas, Dueling network architectures for deep reinforcement learning, in: 33rd Int. Conf. Mach. Learn. ICML 2016 4, 2016, pp. 2939–2947.
- [23] T. Haarnoja, H. Tang, P. Abbeel, S. Levine, Reinforcement learning with deep energy-based policies, in: 34th Int. Conf. Mach. Learn. ICML 2017 3, 2017, pp. 2171–2186.
- [24] D. Silver, G. Lever, N. Heess, T. Degris, D. Wierstra, M. Riedmiller, Deterministic policy gradient algorithms, in: 31st Int. Conf. Mach. Learn. ICML 2014, 1, 2014, pp. 605–619.
- [25] R. Munos, T. Stepleton, A. Harutyunyan, M.G. Bellemare, Safe and efficient off-policy reinforcement learning, in: 30th Conf. Neural Inf. Process. Syst. (NIPS2016), Barcelona, Spain, 2016, pp. 1054–1062.
- [26] J. Schulman, F. Wolski, P. Dhariwal, A. Radford, and O. Klimov, “Proximal policy optimization algorithms,” *arXiv Prepr.*, pp. 1–12, 2017.
- [27] T. Haarnoja et al., “Soft actor-critic algorithms and applications,” *arXiv Prepr.*, pp. 1–17, 2018.
- [28] T. Haarnoja, A. Zhou, P. Abbeel, S. Levine, Soft actor-critic: off-policy maximum entropy deep reinforcement learning with a stochastic actor, in: 35th Int. Conf. Mach. Learn. ICML 2018 5, 2018, pp. 2976–2989.
- [29] P. Christodoulou, “Soft actor-critic for discrete action settings,” *arXiv*, pp. 1–7, 2019.
- [30] J. Duan, Y. Guan, S.E. Li, Y. Ren, Q. Sun, B. Cheng, Distributional soft actor-critic: off-policy reinforcement learning for addressing value estimation errors, *IEEE Trans. Neural Networks Learn. Syst.* (2021) 1–15.
- [31] S. Fujimoto, H. Van Hoof, D. Meger, Addressing function approximation error in actor-critic methods, in: 35th Int. Conf. Mach. Learn. ICML 2018 4, 2018, pp. 2587–2601.
- [32] P. Long, T. Fanl, X. Liao, W. Liu, H. Zhang, J. Pan, Towards optimally decentralized multi-robot collision avoidance via deep reinforcement learning, in: *Proc. - IEEE Int. Conf. Robot. Autom.*, 2018, pp. 6252–6259.
- [33] Y.F. Chen, M. Liu, M. Everett, J.P. How, Decentralized non-communicating multiagent collision avoidance with deep reinforcement learning, in: *Proc. - IEEE Int. Conf. RobotAutom.*, 2017, pp. 285–292.
- [34] C. Zhou, B. Huang, H. Hassan, P. Fränti, Attention-based advantage actor-critic algorithm with prioritized experience replay for complex 2-D robotic motion planning, *J. Intell. Manuf.* 34 (2023) 151–180.
- [35] M. Everett, Y.F. Chen, J.P. How, Motion planning among dynamic, decision-making agents with deep reinforcement learning, in: 2018 IEEE/RSJ Int. Conf. Intell. Robot. Syst. Madrid, Spain, 2018, pp. 3052–3059.
- [36] E. Bas, An introduction to Markov chains, *Basics Probab. Stoch. Process.* (2019) 179–198.
- [37] L. Baird, Residual algorithms: reinforcement learning with function approximation, *Mach. Learn. Proc.* 1995 (1995) 30–37.
- [38] V. Mnih, et al., Human-level control through deep reinforcement learning, *Nature* 518 (7540) (2015) 529–533.
- [39] V.R. Konda, J.N. Tsitsiklis, Actor-critic algorithms, *Adv. Neural Inf. Process. Syst.* (2000) 1008–1014.
- [40] S. Boyd, L. Vandenberghe, *Convex Optimization*, Cambridge Univ. Press, 2004.
- [41] K. He, X. Zhang, S. Ren, J. Sun, Deep residual learning for image recognition, in: *Proc. IEEE Conf. Comput. Vis. Pattern Recognit.*, 2016, pp. 770–778.
- [42] P. Tang, H. Wang, S. Kwong, G-MS2F: goLeNet based multi-stage feature fusion of deep CNN for scene recognition, *Neurocomputing* 225 (2017) 188–197.
- [43] G. Huang, Z. Liu, L. van der Maaten, K.Q. Weinberger, Densely connected convolutional networks, in: *Proc. IEEE Conf. Comput. Vis. Pattern Recognit.*, 2017, pp. 4700–4708.
- [44] K. Xu, S. Jegelka, W. Hu, J. Leskovec, How powerful are graph neural networks?, in: 7th Int. Conf. Learn. Represent. ICLR 2019, 2019, pp. 1–17.
- [45] C. Zhou, C. Wang, H. Hassan, H. Shah, B. Huang, and P. Fränti, “Bayesian inference for data-efficient, explainable, and safe robotic motion planning : a review,” *arXiv: 2307.08024*, pp. 1–33.
- [46] M. Quigley, et al., ROS: an open-source robot operating system, *ICRA Work. open source Softw* 3 (2009) 1–6.
- [47] J.S. Furtado, H.H.T. Liu, G. Lai, H. Lacheray, J. Desouza-Coelho, Comparative analysis of OptiTrack motion capture systems, in: *Proc. Can. Soc. Mech. Eng. Int. Congr.*, Toronto, Canada 2018, 2018. *May* 27–30.
- [48] T. Ameler, et al., A comparative evaluation of SteamVR tracking and the OptiTrack system for medical device tracking, in: *Proc. Annu. Int. Conf. IEEE Eng. Med. Biol. Soc. EMBS*, 2019, pp. 1465–1470.
- [49] V. Garcia-Vázquez, E. Marinetto, J.A. Santos-Miranda, F.A. Calvo, M. Desco, J. Pascau, Feasibility of integrating a multi-camera optical tracking system in intra-operative electron radiation therapy scenarios, *Phys. Med. Biol.* 58 (24) (2013) 8769–8782.
- [50] Y. Xu, D. Hu, L. Liang, S. McAleer, P. Abbeel, and R. Fox, “Target entropy annealing for discrete soft actor-critic,” *arXiv Prepr.*, pp. 1–13, 2021.